Enhancing the efficiency of oncolytic vaccinia virus for ovarian cancer treatment

Stephanie Drymiotou[1], Christophe J. Queval[2], Katherine E. Tyson[3], Lesley A. Sheach[1,†], Antonio Postigo[1,&], Ilaria Dalla Rosa[1], Michael Howell[2], Iain A. McNeish[3]* and Michael Way[1,4]*.

[1]Cellular Signalling and Cytoskeletal Function Laboratory, The Francis Crick Institute, London, NW1 1AT, UK.

[2]High Throughput Screening Laboratory, The Francis Crick Institute.

[3]Ovarian Cancer Action Research Centre, Department of Surgery and Cancer, Imperial College London, W12 0HS, UK

[4]Department of Infectious Disease, Imperial College London, SW7 2AZ, UK.

[†]Current address: Department of Obstetrics & Gynaecology, Barts Health NHS Trust, London, E11 1NR, UK

[&]Current address: Stratosvir Limited, Stevenage Bioscience Catalyst, Stevenage, SG1 2FX, UK

* Joint corresponding authors

Iain McNeish ORCID: 0000-0002-9387-7586

Email: i.mcneish@imperial.ac.uk

Michael Way ORCID: 0000-0001-7207-2722

Email: Michael.Way@crick.ac.uk

Abstract

Vaccinia virus, known for its clinical safety has a tropism for primary and metastatic tumours as well as ovarian tissue. Consequently, oncolytic approaches with recombinant vaccinia viruses have emerged as attractive agents against ovarian cancer. Unfortunately, oncolytic vaccinia monotherapies are yet to live up to their potential promise. Given this, there is a need to identify combination agents that improve the effectiveness of vaccinia in ovarian cancer treatment. We screened 9,000 compounds to identify drugs that enhance the ability of a recombinant vaccinia virus lacking VGF and F1 (ΔVF) to induce death of ID8 *Trp53*$^{-/-}$ murine ovarian cancer cells. We identified a class of tubulin polymerisation inhibitors including vinorelbine. The combination of vinorelbine and vaccinia induces ID8 *Trp53*$^{-/-}$ cell death via apoptosis. In a syngeneic mouse model of high grade serous ovarian carcinoma, ΔVF virus lacking the viral thymidine kinase (TK), armed with GM-CSF and expressing NeonGreen (ΔVFTK-NG-GM-CSF) is tumour specific. A combination of the ΔVFTK-NG-GM-CSF virus with vinorelbine prolongs mouse survival compared to the treatment of mice with either agent alone. Our study suggests vinorelbine is a promising agent to combine with oncolytic vaccinia virus approaches for the management of ovarian cancer.

53 **Introduction**

54 Ovarian cancer (OC) is the sixth most common female malignancy in the UK and the
55 leading cause of death from a gynaecological cancer.[1] It is a highly heterogeneous
56 disease with histotypes varying in their genetic and molecular profiles, clinical phenotypes
57 and risk factors.[2-5] Despite its heterogeneity, standard management has remained the
58 same for decades and includes surgical debulking combined with platinum-taxane
59 chemotherapy.[6-8] Response rates are initially high, especially in high grade serous
60 carcinoma but 80% of patients with advanced disease recur, with all relapsed disease
61 ultimately developing fatal therapy resistance.[9-11] The introduction of bevacizumab (VEGF
62 inhibitor) and PARP inhibitors in treatment regimens based on tumour molecular
63 biomarker status can extend progression-free survival.[12-22] However, the failure of
64 maintenance therapies to extend overall survival for the majority of patients highlights the
65 need for new therapies that overcome chemoresistance.[23]

66

67 Vaccinia virus represents a promising oncolytic agent for OC due to its natural tropism for
68 ovarian tissue.[24-26] The virus is best known for its use as the vaccine for smallpox
69 eradication in the 1980s, demonstrating its safety and tolerability in humans.[27] It also
70 preferentially infects, replicates and kills primary and metastatic tumours over normal
71 tissues.[28-31] This tumour-specific cytotoxicity reduces the systemic side effects induced by
72 the virus compared to existing chemotherapeutics.[32] It also exclusively replicates in the
73 cytoplasm thus avoiding DNA insertions into the host genome.[33, 34] Moreover, the safety
74 and tumour specificity of the virus has been further enhanced through genome
75 manipulation, by deleting genes encoding for virulence factors and proteins regulating
76 nucleotide metabolism.[35] For example, loss of thymidine kinase (TK) and vaccinia growth
77 factor (VGF) significantly reduces viral pathogenicity, reducing side effects in patients,
78 while simultaneously increasing tumour specificity.[26, 36-38] Therefore, TK and VGF are

79 deleted from most vaccinia strains used in clinical trials.[39] Vaccinia can tolerate 25-40 kb
80 foreign DNA insertions and transgenes have been expressed in non-essential loci to
81 improve its oncolytic properties and immunogenicity.[35, 40] Vaccinia kill cells by direct
82 oncolysis and induces immunogenic cell death, an attractive feature that can be exploited
83 and enhanced when used as an oncolytic virus against OC tumours.[41-44]
84
85 Olvi-Vec, derived from the Lister vaccinia strain, is the only oncolytic that has progressed
86 to a phase III clinical trial for the treatment of platinum resistant OC in combination with
87 chemotherapy and bevacizumab.[45, 46] This trial provided evidence that patients with
88 platinum-resistant disease can respond to platinum chemotherapy. In contrast, a phase II
89 clinical trial using the attenuated modified vaccinia Ankara virus expressing 5T4 tumour
90 associated antigen (MVA-5T4, Trovax) monotherapy in asymptomatic women with
91 recurrent ovarian cancer failed to show a significant improvement compared to placebo.[47]
92 This trial highlights the importance of combination therapies for OC with vaccinia.
93
94 The aim of our study was to identify a combination regimen that enhances the efficacy of
95 vaccinia in treating ovarian carcinoma *in vivo.* We took advantage of a recombinant
96 vaccinia virus lacking F1, a viral inhibitor of apoptosis [48, 49] and the vaccinia growth factor
97 (VGF).[50, 51] The recombinant ΔVF virus induces increased cell death during infection
98 compared to the parental Western Reserve (WR).[52] This is the first study in which the
99 oncolytic efficacy of ΔVF was assessed *in vivo* in a syngeneic high grade serous ovarian
100 carcinoma mouse model. Additional recombinant viruses have been constructed to
101 improve the tumour specificity and immunogenicity of ΔVF. A high throughput compound
102 screen was also conducted to identify combination partners that enhance the efficiency of
103 ΔVF and its derivatives in killing ovarian cancer cells and inhibiting tumour progression.
104

105 **Results**

106 **Targeting and arming ΔVF recombinant virus**

107 To improve the potential tumour specificity of the ΔVF virus, we deleted the thymidine
108 kinase (TK) gene to generate the ΔVFTK virus. To facilitate visualisation of infected cells,
109 we also introduced NeonGreen (NG) into the TK locus, generating the ΔVFTK-NG virus.
110 This virus was additionally armed with granulocyte-macrophage colony-stimulating factor
111 (GM-CSF) to enhance its immunogenicity (ΔVFTK-NG-GM-CSF). Characterisation of the
112 new recombinant viruses demonstrated they have similar viral protein expression and
113 spread profiles to the ΔVF virus (Figure 1A and B). Moreover, all viruses retained the pro-
114 apoptotic activity of the parental ΔVF virus (Figure 1C).

115

116 The oncolytic efficacy of the new recombinant viruses was examined *in vivo* using a
117 syngeneic mouse model of high grade serous ovarian carcinoma (ID8 *Trp53*$^{-/-}$) (Figure
118 2A). The heat inactivated ΔVF (ΔVFi) virus was used as vehicle and the median survival
119 of mice in this group was 45.5 days. The median survival of mice inoculated with ΔVF,
120 ΔVFTK, ΔVFTK-NG and ΔVFTK-NG-GM-CSF viruses was 51.5, 51, 51 and 54 days,
121 respectively. Log-rank analysis demonstrated that only ΔVFTK-NG-GM-CSF ($p = 0.005$)
122 significantly prolonged mouse survival (Figure 2B) compared to vehicle control. Viral
123 inoculation of mice with the recombinant viruses had no effect on the size of their liver and
124 spleen nor ascitic volumes (Figure 2C). NeonGreen expression did not affect mouse
125 survival as mice inoculated with ΔVFTK and ΔVFTK-NG had the same median survival of
126 51 days. The *in vivo* experiments indicate the ΔVFTK-NG-GM-CSF virus does improve
127 survival but also illustrates the need to identify combination agents to improve the efficacy
128 of vaccinia virus in ovarian cancer.

129

130

131 **Identifying a combination agent to improve the efficacy of oncolytic vaccinia**

132 A high throughput drug screen was conducted on ΔVFTK-NG infected murine ovarian
133 cancer (ID8 *Trp53*$^{-/-}$) cells (Figure 3A). The library consisted of 9,000 well-characterised
134 compounds that are in clinical development or have been approved by Food and Drug
135 Administration (FDA) and/or European Medicines Agency (EMA) and used in clinic.
136 NeonGreen fluorescence was used to identify infected cells and DAPI staining of nuclei
137 was used to calculate the number of cells remaining at the end of the screen. After imaging
138 of wells compounds were allocated into one of four categories ('no effect', 'kill infected
139 cells', 'block virus replication' and 'toxic') based on the number of infected (green) and
140 uninfected (non-green) cells relative to infected DMSO controls on the same plate (Figure
141 3B). The 'no effect' are wells with similar numbers of infected and uninfected cells
142 compared to the DMSO control, whereas 'block virus replication' are those with reduced
143 infected and increased uninfected cells due to cell proliferation. Toxic compounds resulted
144 in a significant loss of infected and uninfected cells. The ideal compounds are the 'kill
145 infected cells' category as they represent wells with fewer infected but similar numbers of
146 uninfected cells compared to the DMSO control (Figure 3C). These compounds are in
147 principle enhancing the efficacy of vaccinia in killing infected ID8 *Trp53*$^{-/-}$ cells.

148

149 Images from 'kill infected cells' wells were reviewed and a cut-off ratio of infected to
150 uninfected cells of 0.3 was applied to generate the initial hit list of 60 compounds (Table
151 1). During the validation of these hits, an additional 60 compounds, absent from the initial
152 library that belong to the same class of molecules and/or had a similar mechanism of
153 action were added to the hit list (Figure S1). A secondary live-cell imaging screen was
154 conducted to assess compound cytotoxicity as well as the impact on viral replication and
155 spread. Based on this analysis, the compounds were categorised as 'kill infected cells',
156 'impair viral replication' and 'toxic' (Figure 3D). Positive hits ('kill infected cells') were

157 identified based on the reduction in median percentage of infected cell confluency per well
158 over time compared to uninfected cells. This analysis resulted in twenty compounds,
159 seven of which are tubulin polymerisation inhibitors (Figure 3E). We decided to focus on
160 the seven compounds targeting the same process as this is likely to be indicative of true
161 hits.
162
163 Vinorelbine is a semi-synthetic second generation vinca alkaloid with a broad spectrum
164 antitumour activity that inhibits microtubule assembly.[53-55] It has reduced side effects
165 including neurotoxicity compared to other vinca alkaloids.[56-58] An oral vinorelbine
166 formulation is also available making it an appealing combination agent.[55, 59, 60] Vinorelbine
167 is mainly used to treat non-small cell lung and breast cancers but also has some efficacy
168 against ovarian cancer.[61-66] Based on this, we selected vinorelbine for mechanistic
169 exploration and *in vivo* experiments.
170
171 **Vaccinia and vinorelbine induce ID8 *Trp53*$^{-/-}$ cell death via apoptosis**
172 Vinorelbine treatment of uninfected ID8 *Trp53*$^{-/-}$ cells for 16 hours results in the loss of
173 their characteristic cobblestone appearance and cell to cell contacts as well as some cell
174 rounding, indicative of possible progression to cell death (Figure 4A).
175 Immunofluorescence analysis confirmed that vinorelbine results in loss of microtubules in
176 both ID8 *Trp53*$^{-/-}$ cells with or without infection with the ΔVFTK virus (Figure 4B).
177 Vinorelbine treatment also induced nuclear fragmentation and the formation of
178 multinucleated cells suggestive of defects in cytokinesis or cell fusion.
179
180 Vaccinia hijacks the microtubule cytoskeleton to facilitate its replication, intracellular
181 transport and spread.[67-71] We previously found that depolymerization of microtubules with
182 nocodazole reduces virus yield.[72] Consistent with this, immunoblot analysis revealed that

183 vinorelbine treatment reduced both early (F12) and late (F13) viral protein expression, as
184 well as H5, which is required for viral replication (Figure 4C). Vinorelbine treatment prior
185 to infection of ID8 *Trp53*$^{-/-}$ cells clearly impairs viral gene expression but it is not
186 immediately obvious why there is enhanced cell death or which programmed cell death
187 pathway (autophagy, necroptosis or apoptosis) is activated.
188
189 To assess whether vinorelbine induces autophagy in ID8 *Trp53*$^{-/-}$ infected with the ΔVFTK-
190 NG virus, we performed immunoblot analysis to examine the level of p62 expression and
191 LC3 lipidation (LC3-II) (Figure 4D). In contrast to chloroquine treated cells (positive
192 control), there was no change in the level of p62 in infected or non-infected cells with or
193 without vinorelbine. Likewise, the levels of LC3-II did not change, except in the positive
194 control indicating that autophagy is not responsible for increasing cell death of vinorelbine
195 treated ID8 *Trp53*$^{-/-}$ cells.
196
197 To investigate the possible involvement of necroptosis, we performed immunoblot
198 analysis to examine the level of MLKL phosphorylation (pMLKL) and look for the presence
199 of 50 kDa PARP fragment generated by lysosomal proteases.[73, 74] We found pMLKL and
200 the 50 kDa PARP fragment which are indicative of necroptosis are only present in the
201 positive control (0.1% hydrogen peroxide and Z-VAD treatment) (Figure 4E). We did,
202 however, see that vinorelbine induced cleavage of PARP to generate an 89 kDa fragment
203 in infected cells, suggesting that apoptosis is responsible for their death.[75-77] The presence
204 of cleaved caspase 3 and 8 in immunoblots of infected cells treated with vinorelbine
205 confirmed apoptosis was activated (Figure 4F). The combination of vinorelbine and
206 infection is required to induce apoptosis as PARP, caspase 3 or 8 cleavage is not
207 observed in non-infected or infected cells with or without the drug respectively. Pre-
208 treating infected cells with vinorelbine also appears to be more effective at inducing PARP,

209 caspase 3 or 8 cleavage (Figure 4F). To examine if this translates into increased cell death,
210 we performed live cell imaging of ID8 *Trp53*$^{-/-}$ cells treated with vinorelbine before or after
211 vaccinia infection using the same conditions used in the initial drug screen. We found that
212 pre-treating ID8 *Trp53*$^{-/-}$ cells with vinorelbine leads to increased initial cell death
213 compared to adding vinorelbine after infection (Figure 4G). However, both conditions
214 eventually result in similar levels of cell death.
215

216 **Vinorelbine and ΔVFTK-NG-GM-CSF improves mouse survival**

217 An *in vivo* distribution study was carried out to examine the tumour specificity of the
218 ΔVFTK-NG-GM-CSF virus (Figure 5A). Viral replication was detected in omental tumours
219 but not in liver or spleen in mice inoculated intraperitoneally with virus with or without
220 vinorelbine (Figures 5B and C). Pre-treatment with vinorelbine impacted viral replication
221 *in vivo* consistent with our observations in ID8 *Trp53*$^{-/-}$ cells in culture (Figures 5B and D).
222 To assess the efficacy of the combination treatment on the survival of mice we treated
223 mice with vinorelbine 24 hours before injection of the ΔVFTK-NG-GM-CSF virus (Figure
224 5E). This combination prolonged mouse survival compared to vinorelbine (median survival
225 of 73.5 compared to 69 days, $p = 0.022$) (Figure 5F). Moreover, both conditions were also
226 significantly better than virus alone (median 57 days). Our observations suggest that
227 combining vinorelbine and ΔVFTK-NG-GM-CSF virus improves mouse survival against
228 high grade serous ovarian carcinomas.
229

230 **Discussion**

231 Vaccinia virus has the promise of being an ideal oncolytic agent given its safety profile
232 and ability to be genetically enhanced as well as combined with drug treatments.[78, 79]
233 Clinical trials frequently use viruses deleted of genes encoding VGF (ΔVGF) and/or the
234 thymidine kinase (ΔTK) as this increases their tumour specificity and safety.[26, 80] Deletion

235 of F1, an inhibitor of apoptosis in combination with TK also improves the oncolytic
236 effectiveness of the virus as it extends mouse survival in a human glioblastoma model
237 and delays tumour growth in a syngeneic mouse colon model.[48, 49, 81] Based on the
238 available evidence, a virus lacking VGF, TK and F1 is predicted to be safer and induce
239 more tumour cell death.
240
241 We have now deleted VGF, TK and F1 in the Western reserve (WR) strain of Vaccinia
242 and also inserted GM-CSF to the genome to increase the immunogenicity of the virus.
243 NeonGreen was also added which like other reporters, can be used to monitor viral
244 replication, distribution, detect metastatic disease and assess toxicity clinically.[82-85] Our *in*
245 *vivo* survival studies demonstrated that our new recombinant viruses were well tolerated
246 in mice bearing ID8 *Trp53*$^{-/-}$ omental tumours but that only the ΔVFTK-NG-GM-CSF virus
247 had significant survival benefit (Figure 2B). Moreover, when injected intraperitoneally the
248 ΔVFTK-NG-GM-CSF virus specifically replicates in omental tumours but not in the liver or
249 spleen (Figure 5A-C).
250
251 Multiple early phase clinical trials demonstrate that even with genomic modifications that
252 enhance its tumour specificity, oncolytic activity and immunogenicity, vaccinia clearly still
253 needs a combination agent to achieve its full oncolytic potential.[47, 78, 86] Given this, we
254 performed a high throughput drug screen on ID8 *Trp53*$^{-/-}$ cells using 9,000 well-
255 characterised compounds to identify those that increased the killing efficiency of our triple
256 deleted recombinant virus. By performing primary and secondary drug screens, we
257 identified 20 hit compounds, seven of which were tubulin polymerisation inhibitors (Figure
258 3E). Vinorelbine was our drug screen hit compound of choice given it has some activity
259 against ovarian cancer.[61-64]
260

261 We found that the combination of vaccinia with vinorelbine induces ID8 *Trp53*$^{-/-}$ cell death
262 via apoptosis. This is not unexpected, as the ΔVFTK-NG virus lacks F1 the main inhibitor
263 of intrinsic apoptosis during infection.[48, 49] Vinca alkaloids such as vinorelbine also induce
264 apoptosis, which is often attributed to impaired spindle formation and subsequent
265 prolonged mitotic arrest.[87, 88] However, these chemotherapeutics can additionally
266 stimulate apoptosis independently of the cell cycle via alternative mechanisms including
267 the activation of intrinsic apoptosis.[89] Microtubule targeting agents have been shown to
268 upregulate pro-apoptotic Bcl-2 proteins (BAX, BAK, PUMA, Noxa and Bad) as well as
269 inactivate anti-apoptotic Bcl-2 proteins through phosphorylation (Bcl-2, Bcl-xL, Mcl-1, Bcl-
270 W).[87, 90-94] Vinorelbine and the ΔVFTK-NG virus both act on the intrinsic mitochondrial
271 apoptotic pathway and their effects complement each other leading to enhanced apoptotic
272 cell death compared to either agent alone. Therefore, vinorelbine pre-treatment will not
273 only induce mitotic arrest but also activate BAK/BAX leading to mitochondrial membrane
274 pore formation resulting in a pro-apoptotic 'priming' making cells more susceptible to
275 vaccinia induced apoptosis.[95] Consistent with this notion, vinorelbine pre-treatment of
276 cells resulted in increased PARP and caspase cleavage at 24 hours post infection
277 compared to adding the drug after infection (Figure 4F). Live-cell imaging also
278 demonstrated that addition of vinorelbine before infection increased initial cell death
279 compared to first adding the virus and then the drug (Figure 4G).
280
281 When tested in a mouse model of high grade serous ovarian carcinoma, we found that
282 the combination of vinorelbine followed by infection with the ΔVFTK-NG-GM-CSF virus
283 produced a significant survival benefit compared to the control (median survival of 73.5
284 compared to 47.5 days). Our results are in line with previous studies demonstrating that
285 a combination of vinorelbine and vesicular stomatitis virus (VSV) significantly prolonged
286 the survival of aggressive subcutaneous 4T1 syngeneic mouse model of triple negative

287 breast cancer.[96] Vinorelbine has good response rates in phase I and II clinical trials for
288 recurrent ovarian cancer and the National Comprehensive Cancer Network recommended
289 vinorelbine for recurrent epithelial, fallopian tube or primary peritoneal cancers.[8, 61-63] It is
290 evident from our *in vivo* experiments that vinorelbine at the dose used (4mg/kg) has good
291 efficacy against ID8 *Trp53-/-* tumours, suggesting that the drug represents a promising
292 therapy for patients with high grade serous carcinoma. Nevertheless, when vinorelbine is
293 combined with the ΔVFTK-NG-GM-CSF virus mouse survival is further increased. Further
294 experiments are required to examine the impact on mouse survival of reducing the number
295 of doses and concentration of vinorelbine together with higher viral titres. In this way it
296 should be possible to develop strategies with the ΔVFTK-NG-GM-CSF virus that are
297 effective with lower vinorelbine doses to decrease systemic toxicity and the likelihood of
298 patients becoming resistant to vinorelbine.
299
300
301 **Materials and methods**
302 **Cells and culture**
303 The ID8 *Trp53*$^{-/-}$ cell line was provided by Professor Iain McNeish, Imperial College
304 London (London, UK).[97] HeLa and BS-C-1 cell lines were provided by the European
305 Molecular Biology Laboratory (Heidelberg, Germany) and 143B TK$^{-/-}$ from The Francis
306 Crick Institute Cell Services (London, UK). All cell lines were mycoplasma tested and
307 maintained in Dulbecco's Modified Eagle's Medium (DMEM) (Sigma-Aldrich, St. Louis,
308 Missouri, #51435C) supplemented with 10% fetal bovine serum (FBS) (Thermo Fisher
309 Scientific, Waltham, Massachusetts, #10270-106) and 1% penicillin/ streptomycin
310 (pen/strep) (Sigma-Aldrich, #P4333) at 37°C and 5% CO_2.
311
312

313 **Virus amplification and sucrose purification**

314 HeLa cells were grown in 15 cm culture dishes (Corning Inc., Sigma Aldrich, #353025) at
315 approximately 80% confluency and were infected with vaccinia at a MOI of 0.1 for 48-72
316 hours. The cells were scraped in PBS and centrifuged at 500 x g at 4°C for five minutes.
317 Cell pellets were resuspended in PBS and re-centrifuged. The resulting cell pellet was
318 resuspended in 7 ml of Tris buffer (10 mM Tris HCl, 2 mM $MgCl_2$, pH 9.0), disrupted by
319 20 strokes in a 7 ml Wheaton Dounce homogenizer (DWK Life Sciences, Millville, New
320 Jersey, #357538) and centrifuged at 500 x g at 4°C for five minutes. The supernatant was
321 collected and added on top of an 8 ml 35% sucrose cushion in a Beckman SW40
322 ultracentrifuge tube (Beckman Coulter, Brea, California #3117-0380). The solution was
323 centrifuged at 192, 000 x g at 4°C for 30 minutes in a Beckman Optima l-100 XP
324 ultracentrifuge, using an SW32Ti swing-out rotor. The virus pellet was resuspended in a
325 desired amount of Tris buffer, titrated using plaque assays, aliquoted and stored at -20°C
326 (short term) or -80°C (long term).

327

328 **Viral plaque assays and heat inactivation**

329 Confluent monolayers of BS-C-1 cells were infected with vaccinia virus in serum free
330 media at the required dilutions for one hour at 37°C, 5% CO_2. The media was then
331 replaced with 2 ml of semi-solid media (1:1 ratio of 3% Carboxy-methyl cellulose sodium
332 salt dissolved in water and 2X Modified Eagle's Medium (MEM) supplemented with 10%
333 FBS and 1% pen/ strep). After 72 hours, the cells were fixed by adding 1 ml of 8%
334 formaldehyde to the media for 30 minutes at room temperature. The media and
335 formaldehyde were removed, and cells were stained with 1 ml crystal violet (1:5 dilution
336 in Phosphate buffered saline [PBS]) for 30 minutes. Subsequently, the plates were rinsed
337 with cold water and left to air dry. To determine the plaque size, plaque diameter was
338 measured in mm using Fiji line tool, available at imagej.net. For heat inactivation, aliquots

339 of viruses were incubated for three hours at 60°C and then cooled on ice for one hour.
340 Heat inactivation was confirmed by the absence of plaque forming units using plaque
341 assays.
342
343 **Generation of recombinant viruses**
344 Recombinant viruses were constructed in the ΔVF virus background.[52] The transient
345 dominant selection (TDS) method was used to delete TK from the ΔVF genome.[98, 99] To
346 create the targeting vector for TDS a DNA fragment containing the left (387bp) and right
347 (321bp) TK recombination arms was cloned into the pSSGB vector containing the
348 selectable markers GFP-*bsd* under the control of a synthetic vaccinia promoter (pSS). [99]
349 The fluorescent ΔVFTK virus expressing NG (ΔVFTK-NG) and the ΔVFTK virus
350 expressing NG and GM-CSF (ΔVFTK-NG-GM-CSF) under the control of the synthetic
351 early/late vaccinia promoter (pEL) at the TK locus were created via homologous
352 recombination between ΔVF virus and the pBSΔTK-NG and pBSΔTK-NG-GM-CSF
353 targeting vectors, respectively. These targeting vectors were created using BlueScript
354 (PBS(+)) as the backbone vector and DNA fragments containing sequences for pEL-NG
355 and pEL-NG-GM-CSF as the inserts. For all new recombinant viruses, the targeting
356 vectors contained TK recombination arms flanking the DNA sequence to be inserted in
357 the vaccinia genome. A small portion of the 5' open reading frame of J2R (gene encoding
358 for TK) was retained within the left TK recombination arm to ensure the correct
359 transcription of J1R. These DNA fragments were synthesised using the IDT gBlocks gene
360 synthesis service (Coralville, Iowa). Subsequently, HeLa cells, infected with ΔVF at MOI
361 of 0.05 were transfected with the relevant targeting vectors using Lipofectamine 2000
362 (Thermo Fisher Scientific, #52887) and incubated for 48 hours at 37°C and 5% CO_2. The
363 viruses were harvested by scraping the cells and subjecting them to three freeze-thaw
364 cycles. The harvested viruses were used to infect confluent monolayers of 143B $TK^{-/-}$ cells

365 with BrdU selection or BS-C-1 cells with or without blasticidin selection. Recombinant
366 viruses were isolated by identifying and picking fluorescent green plaques over at least
367 three rounds of purification. For all three recombinant viruses, TK deletion and/or
368 insertions of NG or NG-GM-CSF were confirmed by PCR analysis after each round of
369 plaque purification and sequencing. The recombinant viruses were amplified and purified
370 using a 35% sucrose gradient.
371
372 **Quantification of viral DNA**
373 Total DNA was isolated from mouse tissues using DNeasy Blood and Tissue Kit (QIAGEN,
374 Hilden, Germany), as per manufacturer's protocol and quantified using a NanoDrop
375 (Thermo Fisher Scientific). Real-time quantitative PCR (qPCR) was performed in triplicate
376 in 384-well reaction plates (Applied Biosystems, Waltham, Massachusetts). Each PCR
377 reaction (total volume 10 µl) contained 20 ng DNA, 5 µl Power SYBR-Green PCR Master
378 Mix (Applied Biosystems) and 0.5 µM of forward and reverse primers. Viral DNA was
379 amplified using primers specific to a region for H5 vaccinia gene (H5-F: 5'-
380 GTAAGAAGTAAATGCGTGC-3', H5-R: 5'-CCACGTTTGTTCATATACTAC-3') and APP1
381 (APP1-F: 5'-CGGAAACGACGCTCTCATG-3' and APP1-R: 5'-
382 CCAGGCTGAATTCCCCAT-3) was amplified as a nuclear gene standard reference.
383 Changes in viral DNA amount were calculated using the $2^{-\Delta\Delta Ct}$ method and represented
384 as fold changes relative to the indicated control.[100]
385
386 **Immunoblotting**
387 Cells were collected and lysed in 21 µl of PBS supplemented with Protease/ Phosphatase
388 inhibitors (Cell Signalling, #5871) and 5U benzonase nuclease (Millipore, #E1014). SDS
389 was added at a final concentration of 1% followed by 22 µl of 2X SDS loading buffer
390 (Thermo Fisher Scientific, #LC2676). The samples were heated at 95°C for three minutes,

391 loaded onto Bolt 4-12% or 10% Bis-Tris Plus pre-cast gels (Thermo Fisher Scientific) and
392 run in MOPS SDS running buffer (Thermo Fischer Scientific, #NP0001) for 55 minutes at
393 150 V. SeeBluePlus2 protein standard (Thermo Fisher Scientific, #LC5925) was used as
394 reference for protein molecular weight. The proteins were transferred to nitrocellulose
395 membranes (Thermo Fischer Scientific, #IB23001), blocked in 5% milk in PBS with 0.1%
396 Tween20 (PBS-T) (Sigma-Aldrich, #P9416) for one hour at room temperature and
397 incubated overnight with primary antibodies. Primary antibodies used were: F12 (1:4,000,
398 [101]), F13 (1:6,000, [68]), H5 (1:10,000, [102]), GRB2 (1:1,000, Santa Cruz, Dallas, Texas, #sc-
399 255), Vinculin (1:10,000, Sigma-Aldrich, #V9264), GAPDH (1:1,000, Santa Cruz, #sc-
400 32233), PARP (1:1,000, Cell Signalling, Danvers, Massachusetts, #9542), cleaved
401 caspase 8 (1:1,000, Cell Signalling, #8592), cleaved caspase 3 (1:1,000, Cell Signalling,
402 #9664), LC3-B (1:1,000, Abcam [#ab48394], Cambridge, UK) and p62/SQSTM1 (1:1,000,
403 Novus Biologicals, Centennial, Colorado, #NBP1-42822). Goat anti-rabbit (#111035003)
404 and anti-mouse (#115005003) secondary HRP antibodies, obtained from Jackson
405 ImmunoResearch (West Grove, Pennsylvania), were used at 1:10,000 in 5% milk with
406 PBS-T. For the examination of phosphorylated proteins, 1 mM orthovanadate (New
407 England Biolabs, Ipswich, Massachusetts, #P0758) was added during blocking, primary
408 and secondary antibody incubation. The membranes were incubated with SuperSignal
409 West Pico PLUS Chemiluminescence reagent (Thermo Fischer Scientific, #34580) for one
410 minute at room temperature and exposed to UltraCruz Autordiography Film (Santa Cruz,
411 #sc-201697).
412
413 **Drug screen**
414 A small molecule drug library of 9,000 well-characterised compounds, assembled from
415 commercial libraries by the High Throughput Screening (HTS) science technology
416 platform (STP) of the Francis Crick Institute was used for the primary screen. This

417 chemical library can be accessed (https://hts.crick.ac.uk/db/view/libraryView.php) under
418 the database name: 'Full Chemical Collection V6'. A customised library of 120 compounds
419 was purchased form MedChemExpress (Monmouth Junction, New Jersey) for the
420 secondary screen.
421
422 The small molecule library, resuspended in dimethyl sulfoxide (DMSO), was transferred
423 into intermediate Low Dead Volume (LDV; Labcyte, #LPS-0200) 384-well plates at a
424 concentration of 10 and 1 mM. An acoustic liquid handler (Echo 550 Beckman-Coulter)
425 was then used to dispense compounds into Greiner microclear 384-well plates (Greiner,
426 #781091) so they reach a final concentration of 0.1, 1 and 10 μM. Each assay plate was
427 prepared in triplicate. Prior to cell seeding, the compounds were diluted in 10 μl of
428 complete DMEM per well. A volume of 40 μl of cells, corresponding to 3,000 cells, was
429 dispensed into the 384-well assay plates, which were incubated for 16 hours at 5% CO_2
430 and 37°C. The ΔVFTK-NG virus was dispensed in each well at an MOI 0.5 and the plates
431 were incubated at 5% CO_2 and 37°C for 30 hours. Cells were fixed using 4%
432 paraformaldehyde (PFA), permeabilised and stained by adding 0.01% Triton X-100 and
433 DAPI. The cells were imaged on Opera Phenix® Plus (Revvity, Waltham, Massachusetts)
434 using 10x air NA 0.3 objective. The microscope was equipped with a set of lasers and
435 filters for the excitation and emission wavelengths specific for DAPI (excitation: 375 nm
436 and emission: 435-480 nm) and NeonGreen (excitation: 488 nm and emission: 500-550
437 nm).
438
439 **Primary drug screen analysis**
440 Five fields per well were imaged and analysed using Harmony® (version 5.0). Screen data
441 were analysed with the cellHTS2 R package.[103, 104] Raw measurements were scaled

442 relative to the mean of the within-plate DMSO controls to report a percentage-of-control
443 (PoC) for each feature and replicates were summarised as a median value. The replication
444 between technical replicates was assessed using the Spearman correlation. Tibco
445 Spotfire (version 14.0) software was used to process the large datasets. Hit determination
446 was based on how the compounds compared against PoC in terms of infected and
447 uninfected cells.
448
449 **Animal experiments**
450 All animal experiments were carried out in accordance with the UK Home Office
451 regulations under the project licence PA780D61A and PP1321516 (from May 2024) and
452 were approved by the Imperial College Animal Welfare and Ethical Review Body. Female,
453 six- to seven-week-old C57BL/6 mice were purchased from Charles River Laboratories
454 (Harlow, UK) and acclimatised for a week prior to cell injection. They had standard
455 laboratory diet and free access to water. Mice were inoculated intraperitoneally (IP) with
456 ID8 *Trp53*$^{-/-}$ cells ($5x10^6$) in 200 µl sterile PBS on day 0. The tumours were allowed to
457 grow for 14, 21 or 28 days depending on the protocol of each study. Details of the
458 experimental designs of these studies are provided in Figures 1 and 4. Sample sizes were
459 established with the help of the experimental design assistant of NC3Rs to achieve
460 statistical power while minimising animal use. All viruses were injected IP at a titre of $1x10^7$
461 pfu/ml in 200 µl sterile PBS. Vinorelbine tartrate was obtained from Hammersmith hospital
462 pharmacy, Imperial Collage Healthcare NHS Trust (London, UK) and was injected IP at 4
463 mg/kg in 200 µl sterile PBS. The mice were weighed daily, monitored regularly for adverse
464 side effects, and were killed when reached humane endpoints. These included any of the
465 following: swelling restricting movement, piloerection, hunched posture, reduced activity,
466 facial grimace, dehydration lasting > 24 hours, 15% weight loss, altered respiration and
467 self-mutilation. All decisions on animal welfare were made by staff blinded to treatment

468 allocation. The scheduled 1 method followed was cervical dislocation and exsanguination
469 by decapitation. Omental tumours, liver and spleen were dissected and placed in 10%
470 neutral buffered formalin for 48 hours and then transferred to 70% ethanol.
471
472 **Histopathology**
473 Harvested tissues, embedded in paraffin to create blocks, were sectioned at 3 µm
474 thickness and attached on glass microscope slides for examination. Histochemical
475 Haematoxylin and Eosin (H&E) staining was carried out using Tissue-Tek Prisma® *Plus*
476 Automated Slide Stainer (Leica Biosystems, Deer Park, Illinois). Blinded histopathological
477 analysis was performed by Professor Priestnall and Dr Suarez-Bonnet, board-certified
478 veterinary pathologists associated with the Experimental Histopathology STP of The
479 Francis Crick Institute. For immunohistochemistry (IHC), samples were stained for
480 NeonGreen (1:200, Cell Signalling, #41236) and cleaved caspase 3 (1:250, Cell
481 signalling, #9579S) antibodies, respectively. IHC staining was performed on the Leica
482 Bond Rx autostainer platform (Leica Biosystems, #3498240) and a DAB kit which included
483 a secondary antibody, DAB and haematoxylin counterstain was used (BOND Polymer
484 Refine Detection, Leica Biosystems, #DS9800). The slides were scanned with a Zeiss
485 Axio Scan Z1 Slide Scanner operated by ZEN Lite Software.
486
487 **Immunofluorescence**
488 For fixed cell imaging, cells were seeded on 0.1% fibronectin-coated (Sigma-Aldrich,
489 #F0895) coverslips. Cells were infected with vaccinia virus and at experimental endpoint,
490 cells were fixed with 1ml of iced cold methanol for 20 minutes at -20°C and then washed
491 with PBS. Cells were incubated in blocking buffer (1% bovine serum albumin and 2% fetal
492 calf serum) for 30 minutes followed by the primary antibody for one hour. Primary
493 antibodies used were as follows: B5 (1:1,000 [105]) and α - Tubulin (1:500, Sigma-Aldrich,

494 #T6074). Cells were incubated in Alexa Fluor 488 and Alexa Fluor 568 conjugated
495 secondary antibodies (1:1,000 dilution in blocking buffer) for a further 40 minutes and
496 stained with DAPI (300 nM in PBS) for five minutes. Coverslips were mounted on glass
497 microscope slides using 5 µl Mowiol. Mounted coverslips were imaged on a Zeis Axio
498 Observer spinning-disk microscope equipped with a Plan-Apochromat 100x/1.46 oil lens,
499 an Evolve 512 cameral and a Yokagawa CSUX spinning disk. The microscope was
500 controlled by Slidebook software (3i Intelligent Imaging Innovations). Images were
501 analysed using Fiji Imaging Analysis Software.
502
503 **Live-cell imaging**
504 ID8 *Trp53*$^{-/-}$ cells were seeded at the desired confluency in 384-well plates and were
505 transferred to the Incucyte S3 live-cell imaging system (Sartorius) to capture phase-
506 contrast and green-fluorescent images every three hours using a 4x objective. Cells were
507 removed from the Incucyte S3 at the required timepoints for drug treatment and/or
508 infection and quickly replaced in the Incucyte to continue imaging. Whole wells were
509 imaged and analysed using the integrated software module “Basic Analyser”. The median
510 percentage confluency of infected and uninfected cells and the ratio of green fluorescence
511 per well area were quantified. Raw data was exported for further statistical analysis.
512
513 Live cells to assess morphological changes following vinorelbine treatment were imaged
514 using Invitrogen Evos^{TM} M5000 microscope (Invitrogen) equipped with advanced LED
515 illumination and a range of objective lenses to achieve various magnifications. Images
516 were captured using the integrated software.
517
518 **Statistical analysis**

519 Statistical analysis was performed using Prism 10 (GraphPad Software). In all graphs,
520 data are represented by the mean and standard deviations (SD) or median and
521 interquartile range (IQR) from three independent experiments, unless stated otherwise.
522 Data were tested for normality of distribution using normality and lognormality tests in
523 Prism 10. For parametric data: Student's t test was used to compare two data sets and
524 one-way ANOVA for multiple data sets followed by either a Tukey's (comparing samples
525 to each other) or Dunnett's (comparing samples to control) post hoc correction. For non-
526 parametric data: Kruskal Wallis test for multiple data sets followed by Dunn's post hoc
527 test. P values < 0.05 were considered significant. For survival data, Kaplan Meier-survival
528 analysis was used and long-rank Mantel-Cox test was applied to compare two or more
529 survival curves. Pairwise comparisons of individual survival curves were performed
530 manually, and a Bonferroni correction (p value (0.05) / number of comparisons) applied to
531 determine the new threshold of significance.
532
533 **Data availability statement**
534 All data were stored on the internet server of The Francis Crick Institute and can be
535 requested from the corresponding author.
536
537 **Acknowledgments**
538 This project was supported by Cancer Research UK (C422/A29942). M.W. is also
539 supported by the Francis Crick Institute, which receives its core funding from Cancer
540 Research UK (CC2096), the UK Medical Research Council (CC2096), and the Wellcome
541 Trust (CC2096). I.A.M. also acknowledges support from Ovarian Cancer Action (grant
542 number PSN418). For the purpose of open access, the authors have applied a CC BY
543 public copyright licence to any author accepted manuscript version arising from this
544 submission.

545 **Author contributions**

546 **S.D. :**Conceptualization, data curation, formal analysis, investigation, writing - original
547 draft. **C.J.Q. :** Data curation, formal analysis, investigation, methodology, writing – review
548 & editing. **K.E.T. :** *In vivo* investigation, methodology & validation. **L.A.S.:**
549 Conceptualization, writing – review & editing. **A.P. :** Conceptualization, writing – review &
550 editing. **I.D.R. :** Supervision, methodology, writing – review & editing. **M.H. :**Supervision,
551 resources, methodology. **I.A.M. :**Conceptualization, funding acquisition, resources,
552 supervision, writing – review & editing. **M.W. :**Conceptualization, funding acquisition,
553 resources, supervision, writing – review & editing.

554

555 **Declarations of interests**

556 The authors declare no competing interests.

557

558 **Keywords**

559 Vaccinia virus, oncolytic agent, combination therapies, ovarian cancer

560

561

562

563

564

565

566

567

568

569

570

571 **References**

572 1. CRUK. Cancer Research Uk, Ovarian cancer survival statistics 2019 [Available from:
573 https://www.cancerresearchuk.org/health-professional/cancer-statistics/statistics-by-cancer-
574 type/ovarian-cancer/survival#ref-.
575 2. Hollis RL. Molecular characteristics and clinical behaviour of epithelial ovarian cancers.
576 Cancer Lett. 2023;555:216057.
577 3. McCluggage WG, Singh N, Gilks CB. Key changes to the World Health Organization
578 (WHO) classification of female genital tumours introduced in the 5th edition (2020).
579 Histopathology. 2022;80(5):762-78.
580 4. De Leo A, Santini D, Ceccarelli C, Santandrea G, Palicelli A, Acquaviva G, et al. What
581 Is New on Ovarian Carcinoma: Integrated Morphologic and Molecular Analysis Following the
582 New 2020 World Health Organization Classification of Female Genital Tumors. Diagnostics
583 (Basel). 2021;11(4).
584 5. Wentzensen N, Poole EM, Trabert B, White E, Arslan AA, Patel AV, et al. Ovarian
585 Cancer Risk Factors by Histologic Subtype: An Analysis From the Ovarian Cancer Cohort
586 Consortium. J Clin Oncol. 2016;34(24):2888-98.
587 6. Fotopoulou C, Hall M, Cruickshank D, Gabra H, Ganesan R, Hughes C, et al. British
588 Gynaecological Cancer Society (BGCS) epithelial ovarian/fallopian tube/primary peritoneal
589 cancer guidelines: recommendations for practice. Eur J Obstet Gynecol Reprod Biol.
590 2017;213:123-39.
591 7. González-Martín A, Harter P, Leary A, Lorusso D, Miller RE, Pothuri B, et al. Newly
592 diagnosed and relapsed epithelial ovarian cancer: ESMO Clinical Practice Guideline for
593 diagnosis, treatment and follow-up. Ann Oncol. 2023;34(10):833-48.
594 8. Armstrong DK, Alvarez RD, Backes FJ, Bakkum-Gamez JN, Barroilhet L, Behbakht K,
595 et al. NCCN Guidelines® Insights: Ovarian Cancer, Version 3.2022. J Natl Compr Canc Netw.
596 2022;20(9):972-80.

597 9. Hanker LC, Loibl S, Burchardi N, Pfisterer J, Meier W, Pujade-Lauraine E, et al. The
598 impact of second to sixth line therapy on survival of relapsed ovarian cancer after primary
599 taxane/platinum-based therapy. Ann Oncol. 2012;23(10):2605-12.
600 10. Pokhriyal R, Hariprasad R, Kumar L, Hariprasad G. Chemotherapy Resistance in
601 Advanced Ovarian Cancer Patients. Biomark Cancer. 2019;11:1179299x19860815.
602 11. Morgan RD, McNeish IA, Cook AD, James EC, Lord R, Dark G, et al. Objective
603 responses to first-line neoadjuvant carboplatin-paclitaxel regimens for ovarian, fallopian tube,
604 or primary peritoneal carcinoma (ICON8): post-hoc exploratory analysis of a randomised,
605 phase 3 trial. Lancet Oncol. 2021;22(2):277-88.
606 12. Konstantinopoulos PA, Norquist B, Lacchetti C, Armstrong D, Grisham RN, Goodfellow
607 PJ, et al. Germline and Somatic Tumor Testing in Epithelial Ovarian Cancer: ASCO Guideline.
608 J Clin Oncol. 2020;38(11):1222-45.
609 13. Coleman RL, Brady MF, Herzog TJ, Sabbatini P, Armstrong DK, Walker JL, et al.
610 Bevacizumab and paclitaxel-carboplatin chemotherapy and secondary cytoreduction in
611 recurrent, platinum-sensitive ovarian cancer (NRG Oncology/Gynecologic Oncology Group
612 study GOG-0213): a multicentre, open-label, randomised, phase 3 trial. Lancet Oncol.
613 2017;18(6):779-91.
614 14. Ledermann J, Harter P, Gourley C, Friedlander M, Vergote I, Rustin G, et al. Olaparib
615 maintenance therapy in platinum-sensitive relapsed ovarian cancer. New Engl J Med.
616 2012;366(15):1382-92.
617 15. Coleman RL, Oza AM, Lorusso D, Aghajanian C, Oaknin A, Dean A, et al. Rucaparib
618 maintenance treatment for recurrent ovarian carcinoma after response to platinum therapy
619 (ARIEL3): a randomised, double-blind, placebo-controlled, phase 3 trial. Lancet.
620 2017;390(10106):1949-61.
621 16. Mirza MR, Monk BJ, Herrstedt J, Oza AM, Mahner S, Redondo A, et al. Niraparib
622 Maintenance Therapy in Platinum-Sensitive, Recurrent Ovarian Cancer. New Engl J Med.
623 2016;375(22):2154-64.

624 17. Haunschild CE, Tewari KS. Bevacizumab use in the frontline, maintenance and
625 recurrent settings for ovarian cancer. Future Oncol. 2020;16(7):225-46.
626 18. Chan JK, Liu J, Song J, Xiang C, Wu E, Kalilani L, et al. Real-world Outcomes
627 Associated With Poly(ADP-ribose) Polymerase Inhibitor Monotherapy Maintenance in
628 Patients With Primary Advanced Ovarian Cancer. Am J Clin Oncol. 2023;46(7):314-22.
629 19. Pujade-Lauraine E, Hilpert F, Weber B, Reuss A, Poveda A, Kristensen G, et al.
630 Bevacizumab combined with chemotherapy for platinum-resistant recurrent ovarian cancer:
631 The AURELIA open-label randomized phase III trial. J Clin Oncol. 2014;32(13):1302-8.
632 20. Wang L, Wang X, Zhu X, Zhong L, Jiang Q, Wang Y, et al. Drug resistance in ovarian
633 cancer: from mechanism to clinical trial. Mol Cancer. 2024;23(1):66.
634 21. Cordani N, Bianchi T, Ammoni LC, Cortinovis DL, Cazzaniga ME, Lissoni AA, et al. An
635 Overview of PARP Resistance in Ovarian Cancer from a Molecular and Clinical Perspective.
636 Int J Mol Sci. 2023;24(15).
637 22. Haibe Y, Kreidieh M, El Hajj H, Khalifeh I, Mukherji D, Temraz S, et al. Resistance
638 Mechanisms to Anti-angiogenic Therapies in Cancer. Front Oncol. 2020;10:221.
639 23. Vasan N, Baselga J, Hyman DM. A view on drug resistance in cancer. Nature.
640 2019;575(7782):299-309.
641 24. Ascierto ML, Worschech A, Yu Z, Adams S, Reinboth J, Chen NG, et al. Permissivity
642 of the NCI-60 cancer cell lines to oncolytic Vaccinia Virus GLV-1h68. BMC Cancer.
643 2011;11:451.
644 25. Zhao Y, Adams YF, Croft M. Preferential replication of vaccinia virus in the ovaries is
645 independent of immune regulation through IL-10 and TGF-beta. Viral Immunol.
646 2011;24(5):387-96.
647 26. McCart JA, Ward JM, Lee J, Hu Y, Alexander HR, Libutti SK, et al. Systemic cancer
648 therapy with a tumor-selective vaccinia virus mutant lacking thymidine kinase and vaccinia
649 growth factor genes. Cancer Res. 2001;61(24):8751-7.

650 27. Fenner F, Hendersan DA, Arita I, Jezek Z, Ladnyi ID. Smallpox and its eradication:
651 World Health Organisation; 1988.
652 28. Bell J, McFadden G. Viruses for tumor therapy. Cell Host Microbe. 2014;15(3):260-5.
653 29. Yu YA, Shabahang S, Timiryasova TM, Zhang Q, Beltz R, Gentschev I, et al.
654 Visualization of tumors and metastases in live animals with bacteria and vaccinia virus
655 encoding light-emitting proteins. Nat Biotechnol. 2004;22(3):313-20.
656 30. Kirn DH, Thorne SH. Targeted and armed oncolytic poxviruses: a novel multi-
657 mechanistic therapeutic class for cancer. Nat Rev Cancer. 2009;9(1):64-71.
658 31. Parato KA, Breitbach CJ, Le Boeuf F, Wang J, Storbeck C, Ilkow C, et al. The oncolytic
659 poxvirus JX-594 selectively replicates in and destroys cancer cells driven by genetic pathways
660 commonly activated in cancers. Mol Ther. 2012;20(4):749-58.
661 32. Zhang S, Rabkin SD. The discovery and development of oncolytic viruses: are they
662 the future of cancer immunotherapy? Expert Opin Drug Discov. 2021;16(4):391-410.
663 33. Moss B. Poxvirus DNA replication. Cold Spring Harb Perspect Biol. 2013;5(9).
664 34. Li M, Zhang M, Ye Q, Liu Y, Qian W. Preclinical and clinical trials of oncolytic vaccinia
665 virus in cancer immunotherapy: a comprehensive review. Cancer Biol Med. 2023;20(9):646-
666 61.
667 35. Guo ZS, Lu B, Guo Z, Giehl E, Feist M, Dai E, et al. Vaccinia virus-mediated cancer
668 immunotherapy: cancer vaccines and oncolytics. J Immunother Cancer. 2019;7(1):6.
669 36. Buller RM, Smith GL, Cremer K, Notkins AL, Moss B. Decreased virulence of
670 recombinant vaccinia virus expression vectors is associated with a thymidine kinase-negative
671 phenotype. Nature. 1985;317(6040):813-5.
672 37. Byrd CM, Hruby DE. Construction of Recombinant Vaccinia Virus. In: Isaacs SN, editor.
673 Vaccinia Virus and Poxvirology: Methods and Protocols. Totowa, NJ: Humana Press; 2004.
674 p. 31-40.
675 38. Hruby DE, Ball LA. Control of expression of the vaccinia virus thymidine kinase gene.
676 J Virol. 1981;40(2):456-64.

677 39. Zhang Z, Dong L, Zhao C, Zheng P, Zhang X, Xu J. Vaccinia virus-based vector
678 against infectious diseases and tumors. Hum Vaccin Immunother. 2021;17(6):1578-85.
679 40. Smith GL, Moss B. Infectious poxvirus vectors have capacity for at least 25 000 base
680 pairs of foreign DNA. Gene. 1983;25(1):21-8.
681 41. Chiocca EA, Rabkin SD. Oncolytic viruses and their application to cancer
682 immunotherapy. Cancer Immunol Res. 2014;2(4):295-300.
683 42. Kaufman HL, Kohlhapp FJ, Zloza A. Oncolytic viruses: a new class of immunotherapy
684 drugs. Nat Rev Drug Discov. 2015;14(9):642-62.
685 43. Gujar S, Pol JG, Kim Y, Lee PW, Kroemer G. Antitumor Benefits of Antiviral Immunity:
686 An Underappreciated Aspect of Oncolytic Virotherapies. Trends Immunol. 2018;39(3):209-21.
687 44. Gujar S, Pol JG, Kroemer G. Heating it up: Oncolytic viruses make tumors 'hot' and
688 suitable for checkpoint blockade immunotherapies. Oncoimmunology. 2018;7(8):e1442169.
689 45. Holloway RW, Thaker P, Mendivil AA, Ahmad S, Al-Niaimi AN, Barter J, et al. A phase
690 III, multicenter, randomized study of olvimulogene nanivacirepvec followed by platinum-
691 doublet chemotherapy and bevacizumab compared with platinum-doublet chemotherapy and
692 bevacizumab in women with platinum-resistant/refractory ovarian cancer. Int J Gynecol
693 Cancer. 2023;33(9):1458-63.
694 46. Holloway RW, Mendivil AA, Kendrick JE, Abaid LN, Brown JV, LeBlanc J, et al. Clinical
695 Activity of Olvimulogene Nanivacirepvec–Primed Immunochemotherapy in Heavily Pretreated
696 Patients With Platinum-Resistant or Platinum-Refractory Ovarian Cancer: The
697 Nonrandomized Phase 2 VIRO-15 Clinical Trial. JAMA Oncol. 2023;9(7):903-8.
698 47. Michael A, Wilson W, Sunshine S, Annels N, Harrop R, Blount D, et al. A randomized
699 phase II trial to examine modified vaccinia Ankara-5T4 vaccine in patients with relapsed
700 asymptomatic ovarian cancer (TRIOC). Int J Gynecol Cancer. 2024.
701 48. Postigo A, Cross JR, Downward J, Way M. Interaction of F1L with the BH3 domain of
702 Bak is responsible for inhibiting vaccinia-induced apoptosis. Cell Death Differ.
703 2006;13(10):1651-62.

704 49. Wasilenko ST, Banadyga L, Bond D, Barry M. The vaccinia virus F1L protein interacts
705 with the proapoptotic protein Bak and inhibits Bak activation. J Virol. 2005;79(22):14031-43.
706 50. Blomquist MC, Hunt LT, Barker WC. Vaccinia virus 19-kilodalton protein: relationship
707 to several mammalian proteins, including two growth factors. Proc Natl Acad Sci U S A.
708 1984;81(23):7363-7.
709 51. Brown JP, Twardzik DR, Marquardt H, Todaro GJ. Vaccinia virus encodes a
710 polypeptide homologous to epidermal growth factor and transforming growth factor. Nature.
711 1985;313(6002):491-2.
712 52. Postigo A, Martin MC, Dodding MP, Way M. Vaccinia-induced epidermal growth factor
713 receptor-MEK signalling and the anti-apoptotic protein F1L synergize to suppress cell death
714 during infection. Cell Microbiol. 2009;11(8):1208-18.
715 53. Gregory RK, Smith IE. Vinorelbine--a clinical review. Br J Cancer. 2000;82(12):1907-
716 13.
717 54. Banyal A, Tiwari S, Sharma A, Chanana I, Patel SKS, Kulshrestha S, et al. Vinca
718 alkaloids as a potential cancer therapeutics: recent update and future challenges. 3 Biotech.
719 2023;13(6):211.
720 55. Rowinsky EK, Donehower RC. The clinical pharmacology and use of antimicrotubule
721 agents in cancer chemotherapeutics. Pharmacol Ther. 1991;52(1):35-84.
722 56. Galano G, Caputo M, Tecce MF, Capasso A. Efficacy and tolerability of vinorelbine in
723 the cancer therapy. Curr Drug Saf. 2011;6(3):185-93.
724 57. Martino E, Casamassima G, Castiglione S, Cellupica E, Pantalone S, Papagni F, et al.
725 Vinca alkaloids and analogues as anti-cancer agents: Looking back, peering ahead. Bioorg
726 Med Chem Lett. 2018;28(17):2816-26.
727 58. Johnson SA, Harper P, Hortobagyi GN, Pouillart P. Vinorelbine: an overview. Cancer
728 Treatment Reviews. 1996;22(2):127-42.

729 59. Gralla RJ, Gatzemeier U, Gebbia V, Huber R, O'Brien M, Puozzo C. Oral vinorelbine
730 in the treatment of non-small cell lung cancer: rationale and implications for patient
731 management. Drugs. 2007;67(10):1403-10.
732 60. Barletta G, Genova C, Rijavec E, Burrafato G, Biello F, Sini C, et al. Oral vinorelbine
733 in the treatment of non-small-cell lung cancer. Expert Opin Pharmacother. 2014;15(11):1585-
734 99.
735 61. Rothenberg ML, Liu PY, Wilczynski S, Nahhas WA, Winakur GL, Jiang CS, et al.
736 Phase II trial of vinorelbine for relapsed ovarian cancer: a Southwest Oncology Group study.
737 Gynecol Oncol. 2004;95(3):506-12.
738 62. Bajetta E, Di Leo A, Biganzoli L, Mariani L, Cappuzzo F, Di Bartolomeo M, et al. Phase
739 II study of vinorelbine in patients with pretreated advanced ovarian cancer: activity in platinum-
740 resistant disease. J Clin Oncol. 1996;14(9):2546-51.
741 63. Yeon SH, Lee MW, Ryu H, Song IC, Yun HJ, Jo DY, et al. Efficacy of cisplatin
742 combined with vinorelbine as second- or higher-line palliative chemotherapy in patients with
743 advanced ovarian cancer. Medicine (Baltimore). 2023;102(11):e33271.
744 64. Sørensen P, Høyer M, Jakobsen A, Malmström H, Havsteen H, Bertelsen K. Phase II
745 study of vinorelbine in the treatment of platinum-resistant ovarian carcinoma. Gynecol Oncol.
746 2001;81(1):58-62.
747 65. NICE. Vinorelbine 2024 [
748 66. Xu YC, Wang HX, Tang L, Ma Y, Zhang FC. A systematic review of vinorelbine for the
749 treatment of breast cancer. Breast J. 2013;19(2):180-8.
750 67. Dodding MP, Way M. Coupling viruses to dynein and kinesin-1. EMBO J.
751 2011;30(17):3527-39.
752 68. Rietdorf J, Ploubidou A, Reckmann I, Holmström A, Frischknecht F, Zettl M, et al.
753 Kinesin-dependent movement on microtubules precedes actin-based motility of vaccinia virus.
754 Nat Cell Biol. 2001;3(11):992-1000.

755 69. Ploubidou A, Way M. Viral transport and the cytoskeleton. Curr Opin Cell Biol.
756 2001;13(1):97-105.
757 70. Leite F, Way M. The role of signalling and the cytoskeleton during Vaccinia Virus
758 egress. Virus Res. 2015;209:87-99.
759 71. Xu A, Basant A, Schleich S, Newsome TP, Way M. Kinesin-1 transports
760 morphologically distinct intracellular virions during vaccinia infection. J Cell Sci. 2023;136(5).
761 72. Ploubidou A, Moreau V, Ashman K, Reckmann I, González C, Way M. Vaccinia virus
762 infection disrupts microtubule organization and centrosome function. EMBO J.
763 2000;19(15):3932-44.
764 73. Gobeil S, Boucher CC, Nadeau D, Poirier GG. Characterization of the necrotic
765 cleavage of poly(ADP-ribose) polymerase (PARP-1): implication of lysosomal proteases. Cell
766 Death Differ. 2001;8(6):588-94.
767 74. Shah GM, Shah RG, Poirier GG. Different cleavage pattern for poly(ADP-ribose)
768 polymerase during necrosis and apoptosis in HL-60 cells. Biochem Biophys Res Commun.
769 1996;229(3):838-44.
770 75. Kaufmann SH, Desnoyers S, Ottaviano Y, Davidson NE, Poirier GG. Specific
771 proteolytic cleavage of poly(ADP-ribose) polymerase: an early marker of chemotherapy-
772 induced apoptosis. Cancer Res. 1993;53(17):3976-85.
773 76. Kaufmann SH. Induction of endonucleolytic DNA cleavage in human acute
774 myelogenous leukemia cells by etoposide, camptothecin, and other cytotoxic anticancer
775 drugs: a cautionary note. Cancer Res. 1989;49(21):5870-8.
776 77. Lazebnik YA, Kaufmann SH, Desnoyers S, Poirier GG, Earnshaw WC. Cleavage of
777 poly(ADP-ribose) polymerase by a proteinase with properties like ICE. Nature.
778 1994;371(6495):346-7.
779 78. Mirbahari SN, Da Silva M, Zúñiga AIM, Kooshki Zamani N, St-Laurent G, Totonchi M,
780 et al. Recent progress in combination therapy of oncolytic vaccinia virus. Front Immunol.
781 2024;15.

782 79. Xu L, Sun H, Lemoine NR, Xuan Y, Wang P. Oncolytic vaccinia virus and cancer
783 immunotherapy. Front Immunol. 2024;14.
784 80. Buller RM, Chakrabarti S, Cooper JA, Twardzik DR, Moss B. Deletion of the vaccinia
785 virus growth factor gene reduces virus virulence. J Virol. 1988;62(3):866-74.
786 81. Pelin A, Foloppe J, Petryk J, Singaravelu R, Hussein M, Gossart F, et al. Deletion of
787 Apoptosis Inhibitor F1L in Vaccinia Virus Increases Safety and Oncolysis for Cancer Therapy.
788 Mol Ther Oncolytics. 2019;14:246-52.
789 82. Haddad D, Fong Y. Molecular imaging of oncolytic viral therapy. Mol Ther Oncolytics.
790 2015;1:14007.
791 83. Kelly KJ, Wong J, Gönen M, Allen P, Brennan M, Coit D, et al. Human Trial of a
792 Genetically Modified Herpes Simplex Virus for Rapid Detection of Positive Peritoneal Cytology
793 in the Staging of Pancreatic Cancer. EBioMedicine. 2016;7:94-9.
794 84. Miller A, Russell SJ. The use of the NIS reporter gene for optimizing oncolytic
795 virotherapy. Expert Opin Biol Ther. 2016;16(1):15-32.
796 85. Concilio SC, Russell SJ, Peng KW. A brief review of reporter gene imaging in oncolytic
797 virotherapy and gene therapy. Mol Ther Oncolytics. 2021;21:98-109.
798 86. Abou-Alfa GK, Galle PR, Chao Y, Erinjeri J, Heo J, Borad MJ, et al. PHOCUS: A Phase
799 3, Randomized, Open-Label Study of Sequential Treatment with Pexa-Vec (JX-594) and
800 Sorafenib in Patients with Advanced Hepatocellular Carcinoma. Liver Cancer.
801 2024;13(3):248-64.
802 87. Bates D, Eastman A. Microtubule destabilising agents: far more than just antimitotic
803 anticancer drugs. Br J Clin Pharmacol. 2017;83(2):255-68.
804 88. Rieder CL, Maiato H. Stuck in Division or Passing through: What Happens When Cells
805 Cannot Satisfy the Spindle Assembly Checkpoint. Dev Cell. 2004;7(5):637-51.
806 89. Rovini A, Savry A, Braguer D, Carré M. Microtubule-targeted agents: when
807 mitochondria become essential to chemotherapy. Biochim Biophys Acta. 2011;1807(6):679-
808 88.

809 90. Whitaker RH, Placzek WJ. Regulating the BCL2 Family to Improve Sensitivity to
810 Microtubule Targeting Agents. Cells. 2019;8(4).
811 91. Pourroy B, Carré M, Honoré S, Bourgarel-Rey V, Kruczynski A, Briand C, et al. Low
812 concentrations of vinflunine induce apoptosis in human SK-N-SH neuroblastoma cells through
813 a postmitotic G1 arrest and a mitochondrial pathway. Mol Pharmacol. 2004;66(3):580-91.
814 92. Pathan N, Aime-Sempe C, Kitada S, Haldar S, Reed JC. Microtubule-targeting drugs
815 induce Bcl-2 phosphorylation and association with Pin1. Neoplasia. 2001;3(1):70-9.
816 93. Wordeman L, Vicente JJ. Microtubule Targeting Agents in Disease: Classic Drugs,
817 Novel Roles. Cancers. 2021;13(22).
818 94. Yamaguchi H, Chen J, Bhalla K, Wang H-G. Regulation of Bax activation and apoptotic
819 response to microtubule-damaging agents by p53 transcription-dependent and-independent
820 pathways. J Biol Chem. 2004;279(38):39431-7.
821 95. Ni Chonghaile T, Sarosiek KA, Vo TT, Ryan JA, Tammareddi A, Moore Vdel G, et al.
822 Pretreatment mitochondrial priming correlates with clinical response to cytotoxic
823 chemotherapy. Science. 2011;334(6059):1129-33.
824 96. Arulanandam R, Batenchuk C, Varette O, Zakaria C, Garcia V, Forbes NE, et al.
825 Microtubule disruption synergizes with oncolytic virotherapy by inhibiting interferon translation
826 and potentiating bystander killing. Nat Commun. 2015;6:6410.
827 97. Walton J, Blagih J, Ennis D, Leung E, Dowson S, Farquharson M, et al. CRISPR/Cas9-
828 Mediated Trp53 and Brca2 Knockout to Generate Improved Murine Models of Ovarian High-
829 Grade Serous Carcinoma. Cancer Res. 2016;76(20):6118-29.
830 98. Falkner FG, Moss B. Transient dominant selection of recombinant vaccinia viruses. J
831 Virol. 1990;64(6):3108-11.
832 99. Wong YC, Lin LC, Melo-Silva CR, Smith SA, Tscharke DC. Engineering recombinant
833 poxviruses using a compact GFP-blasticidin resistance fusion gene for selection. J Virol
834 Methods. 2011;171(1):295-8.

835 100. Schmittgen TD, Livak KJ. Analyzing real-time PCR data by the comparative C(T)
836 method. Nat Protoc. 2008;3(6):1101-8.
837 101. Dodding MP, Newsome TP, Collinson LM, Edwards C, Way M. An E2-F12 complex is
838 required for intracellular enveloped virus morphogenesis during vaccinia infection. Cell
839 Microbiol. 2009;11(5):808-24.
840 102. Tolonen N, Doglio L, Schleich S, Krijnse Locker J. Vaccinia virus DNA replication
841 occurs in endoplasmic reticulum-enclosed cytoplasmic mini-nuclei. Mol Biol Cell.
842 2001;12(7):2031-46.
843 103. End-to-end analysis of cell-based screens: from raw intensity readings to the
844 annotated hit list. [Internet]. 2023 [cited April 2024]. Available from:
845 https://bioconductor.org/packages/release/bioc/vignettes/cellHTS2/inst/doc/cellhts2Complete
846 .pdf.
847 104. Boutros M, Brás LP, Huber W. Analysis of cell-based RNAi screens. Genome Biol.
848 2006;7(7):R66.
849 105. Schmelz M, Sodeik B, Ericsson M, Wolffe EJ, Shida H, Hiller G, et al. Assembly of
850 vaccinia virus: the second wrapping cisterna is derived from the trans Golgi network. J Virol.
851 1994;68(1):130-47.
852

853 **Figure legends**

854 **Figure 1. Characterisation of recombinant vaccinia viruses**

855 **A**. Immunoblot analysis comparing the expression levels of the indicated viral proteins in HeLa
856 cells infected with the indicated viruses (MOI of 1) at 4 and 8 hpi. Vinculin is the cell loading
857 control and NeonGreen is only detected in ΔVFTK-NG and ΔVFTK-NG-GM-CSF infected
858 cells. The experiment was repeated three times and a representative example is shown. **B.**
859 Representative images of plaque formation by the indicated virus strains in BS-C-1 cells at 72
860 hpi. The graph represents quantitative analysis of plaque diameter measured in mm for the
861 indicated viral strains. The three independent plaque assays are represented by the three

862 different colours in the SuperPlot. Each dot represents one plaque, and the triangles represent
863 the medians of all the plaques measured in each experiment. Data are represented as mean
864 ± SD. One-way ANOVA was used to determine significance between all groups with Tukey
865 multiple comparisons post-hoc test. **C**. Immunoblot analysis reveals increased PARP
866 cleavage following infection of ID8 *Trp53*$^{-/-}$ cells with ΔVF, ΔVFTK, ΔVFTK-NG, ΔVFTK-NG-
867 GM-CSF compared to WR after 48 hours. F12 and GRB2 represent viral and cell loading
868 controls respectively. The asterisk (*) indicates a non-specific band. Hpi = hours post infection.
869 The experiment was repeated three times and a representative blot is shown.
870
871 **Figure 2. Efficacy of recombinant vaccinia viruses in vivo**
872 **A.** Schematic representation of the experimental design of the *in vivo* survival study. Five
873 groups of mice were injected IP with ID8 *Trp53*$^{-/-}$ cells on day 0 and subsequently inoculated
874 with the indicated viruses on day 21, 28 and 35. ΔVFi is the control heat inactivated virus. **B.**
875 Kaplan-Meier survival curve showing survival data for each virus analysed by log-rank test. **C.**
876 Quantification of omental tumour, spleen and liver weights as well as ascitic volumes for each
877 group. Data are represented as mean ± SD. One-way ANOVA was used to determine
878 significance between all groups with Tukey multiple comparisons post-hoc test.
879
880 **Figure 3. Identifying targets for combination therapies with oncolytic vaccinia**.
881 **A.** Schematic summarising the high throughput drug screening strategy. **B.** Representative
882 images of ID8 *Trp53*$^{-/-}$ cells infected with ΔVFTK-NG virus and treated with the indicated
883 compounds belonging to the four categories. NeonGreen expression (green) indicates
884 infected cells and DAPI was used to stain nuclei (blue). Cells were imaged using Opera Phenix
885 Plus with 10x air objective. Scale bar = 200 μm. **C.** Graphical illustration of compound
886 allocation in the four categories. **D.** Representative graphs from the secondary validation
887 screen of selected primary screen hits at 1μM (omipalisib, erlotinib and vinorelbine). The
888 model represents an ideal compound and DMSO is the negative control. The purple dashed

889 line represents the time at which ΔVFTK-NG virus (MOI 0.5) was added (16 hours post cell
890 seeding). Statistical analysis was done by comparing uninfected against infected cell
891 confluency at 20, 60 and 90 hours post cell seeding using Student's t-test. Error bars represent
892 standard deviation (SD). **E.** List of hit compounds after the secondary validation screen.
893
894 **Figure 4. Vaccinia and vinorelbine induces apoptotic ID8 *Trp53*$^{-/-}$ cell death**
895 **A.** Representative phase contrast images of ID8 *Trp53*$^{-/-}$ cells after 16 hours treatment with
896 DMSO or vinorelbine (1 μM). Scale bar = 150 μm. **B.** Immunofluorescent images of
897 microtubule cytoskeleton (Tubulin - green) in ID8 *Trp53*$^{-/-}$ cells treated with DMSO or
898 vinorelbine with or without infection with ΔVFTK (Vaccinia - red). DAPI (blue) was used to
899 stain nuclei and cytoplasmic viral factories. Yellow arrows indicate fragmented nuclei. Scale
900 bar = 10 μM. **C.** Immunoblot of the indicated viral proteins following infection for 4 or 8 hours
901 with ΔVFTK-NG following 16 hours pre-treatment with DMSO or vinorelbine. Vinculin is the
902 cell loading control. **D.** Immunoblot examining the levels of LC3 lipidation (LC3-II) and p62 in
903 ID8 *Tr53*$^{-/-}$ cells pretreated with vinorelbine or DMSO for 8 hours and infected with ΔVFTK-NG
904 for 24 hours. Chloroquine (Clq) treatment for 3 hours represents the positive control. **E.**
905 Immunoblot examining the levels pf MLKL phosphorylation and PARP cleavage in ID8 *Tr53*$^{-/-}$
906 cells pretreated with vinorelbine or DMSO for 8 hours and infected with ΔVFTK-NG for 24
907 hours. Staurosporine (S) (8 hours) and 0.1% hydrogen peroxide (H_2O_2) combined with Z-VAD
908 (two hours) represent positive controls for apoptosis and necroptosis respectively. **F.**
909 Immunoblot examining the levels of cleaved caspase 8, 3 and PARP in ID8 *Tr53*$^{-/-}$ cells treated
910 with vinorelbine 8 hours before or after infection with ΔVFTK-NG for 24 hours. In D, E and F
911 H5 and GAPDH repsent the viral and cell loading controls, respectively. For all experiments,
912 uninfected DMSO-treated cells (UI) were the negative control. Asterisks (*) indicate non-
913 specific bands. Immunoblot experiments were repeated three times and representative
914 examples are shown. **G.** Median percentage cell confluency over time for the indicated
915 conditions. Cells were treated with the indicated compounds or ΔVFTK-NG at 16 hours post

916 seeding (dashed line numbered 1). The dashed line numbered 2 (24 hours post cell seeding)
917 represents the time of addition of either vinorelbine or ΔVFTK-NG for the combination groups.
918
919 **Figure 5. Assessing the efficacy of ΔVFTK-NG-GM-CSF in vivo**
920 **A.** Schematic representation of the experimental design of the distribution study. Mice were
921 injected IP with ID8 *Trp53*$^{-/-}$ cells on day 0 and received their IP injection on day 28 and the
922 combination groups received their second component (vinorelbine or virus) on day 29. Heat
923 inactivated (HI) virus (ΔVFTK-NG-GM-CSFi) is the negative control. **B.** Quantification of viral
924 DNA in omental tumour, liver and spleen measured by qPCR and expressed relative to viral
925 DNA levels of the liver sample in the HI virus group. Error bars represent mean ± SD. **C.**
926 Representative immunohistochemical images of the distribution of cleaved caspase 3 and
927 NeonGreen in omental tumour, liver and spleen harvested from a mouse in Group 4. **D.**
928 Representative immunohistochemical images of the distribution of cleaved caspase 3 and
929 NeonGreen in omental tumours from mice in Groups 1, 3 and 4. **E.** Schematic representation
930 of the experimental design of the vaccinia-vinorelbine combination study. Mice were injected
931 with ID8 *Trp53*$^{-/-}$ cells on day 0 and started receiving their IP treatment injections on day 21.
932 Mice allocated to single treatment groups received their inoculations on days 21, 28 and 35
933 and those allocated to the combination groups received vinorelbine and ΔVFTK-NG-GM-CSF
934 24 hours apart. Heat inactivated (HI) ΔVFTK-NG-GM-CSFi virus was the negative control. **F.**
935 Kaplan-Meier survival curve showing survival data for each group analysed by log-rank test.
936 One mice belonging to group 2 was excluded from the analysis as after IP injection of ID8
937 *Trp53* $^{-/-}$ cells omental tumour failed to form. The analysis is from the combination of two
938 survival experiments following the same protocols.
939
940
941
942 **Table 1. List of 60 primary screen hits**

Drug	Mechanism of Action
2-amino-8-[4-(2-hydroxyethoxy) cyclohexyl]-6-(6-methoxy-3-pyridinyl)-4-methylpyrido[2,3-d]pyrimidin-7(8H)-one	PI3K/mTOR kinase inhibitor
5-Fluorouridine	Pyrimidine nucleoside analogue
Abexinostat	Pan-histone deacetylase inhibitor
Actinomycin	DNA repair inhibitor
Alvespimycin (17-DMAG) hydrochloride	HSP 90 inhibitor
Aminopterin	Dihydrofolate reductase inhibitor
Amsacrine hydrochloride	Topoisomerase II inhibitor
AT13387	HSP 90 inhibitor
Auristatin F	Tubulin polymerisation inhibitor
Bortezomib	Proteosome inhibitor
Canertinib	EGFR inhibitor
CCT137690	Aurora kinase inhibitor
Cephaeline	Emetic alkaloid
CH5138303	HSP 90 inhibitor
CHIR-124	Selective Chk1 inhibitor
Chromomycin A3	DNA replication and transcription inhibitor
Combretastatin A4	Tubulin polymerisation inhibitor
Cytarabine	Pyrimidine nucleoside analogue
Cytochalasin E	Actin polymerisation inhibitor
D8-MMAD	Tubulin polymerisation inhibitor
D8-MMAF hydrochloride	Tubulin polymerisation inhibitor
Diacetoxyscirpenol	Ribosome inhibitor
Diosgenin	Precursor of steroidal hormones
Dp44mT	Iron chelator
Ellipticine	Topoisomerase II inhibitor
Emetine hydrochloride hydrate	Ribosome inhibitor
Enzastaurin	Protein kinase C inhibitor
Erastin	Ferroptosis inhibitor
Ergosterol	Sterol
Floxuridine	Pyrimidine nucleoside analogue
Fosbretabulin disodium	Tubulin polymerisation inhibitor
Ganetespib	HSP90 inhibitor
Geldanamycin	HSK90 inhibitor
Gemcitabine	Nucleoside (cytidine analogue) metabolic inhibitor
GSK3787	PPARδ antagonist
HSP990	HSP90 inhibitor
Imidazole ketone erastin	Ferroptosis inhibitor
MMAD	Tubulin polymerisation inhibitor
MMAF hydrochloride	Tubulin polymerisation inhibitor
MMAF-OMe	ADC cytotoxin and tubulin polymerisation inhibitor
NSC319726	$p53^{R175}$ mutant reactivator
Nutlin-3	P53-MDM2 interaction inhibitor
NVP-TAE226	Focal adhesion kinase inhibitor
Pazopanib hydrochloride	Protein tyrosine kinase inhibitor
PDGF receptor tyrosine kinase inhibitor IV	Tyrosine kinase inhibitor
Premetrexed	Folate-dependent enzyme inhibitor. Inhibitor of nucleotide synthesis
Podophyllotoxin	Tubulin polymerisation inhibitor
Pralatrexate	Dihydrofolate reductase inhibitor
PU-H71	HSP90 inhibitor
Raltitrexed	Thymidylate synthase inhibitor
Rosiglitazone	PPAR agonist
Silvestrol	RNA helicase inhibitor
Tanespimycin	HSP90 inhibitor
Thapsigargin	Sarco-endoplasmic reticulum Ca^{2+} ATPase inhibitor
TRAM-34	Potassium Channel inhibitor
Trifluridine	Nucleoside metabolic inhibitor
Tubulin inhibitor 1	Tubulin polymerisation inhibitor
Vinblastine	Tubulin polymerisation inhibitor
Vincristine sulfate	Tubulin polymerisation inhibitor
Vinorelbine	Tubulin polymerisation inhibitor

943

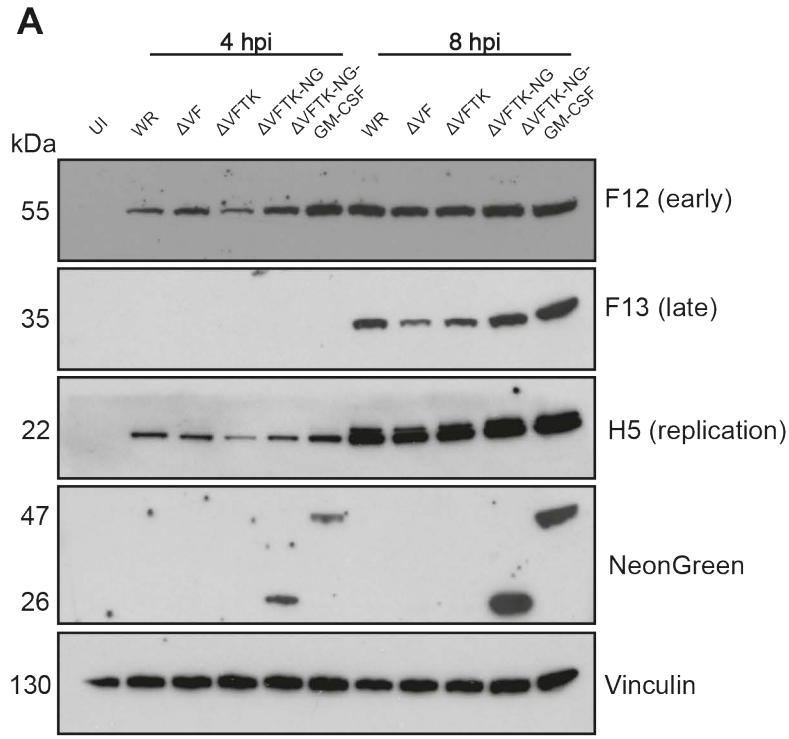
A
4 hpi
8 hpi
kDa
UI
WR
ΔVF
ΔVFTK
ΔVFTK-NG
ΔVFTK-NG-GM-CSF
WR
ΔVF
ΔVFTK
ΔVFTK-NG
ΔVFTK-NG-GM-CSF
55
F12 (early)
35
F13 (late)
22
H5 (replication)
47
26
NeonGreen
130
Vinculin

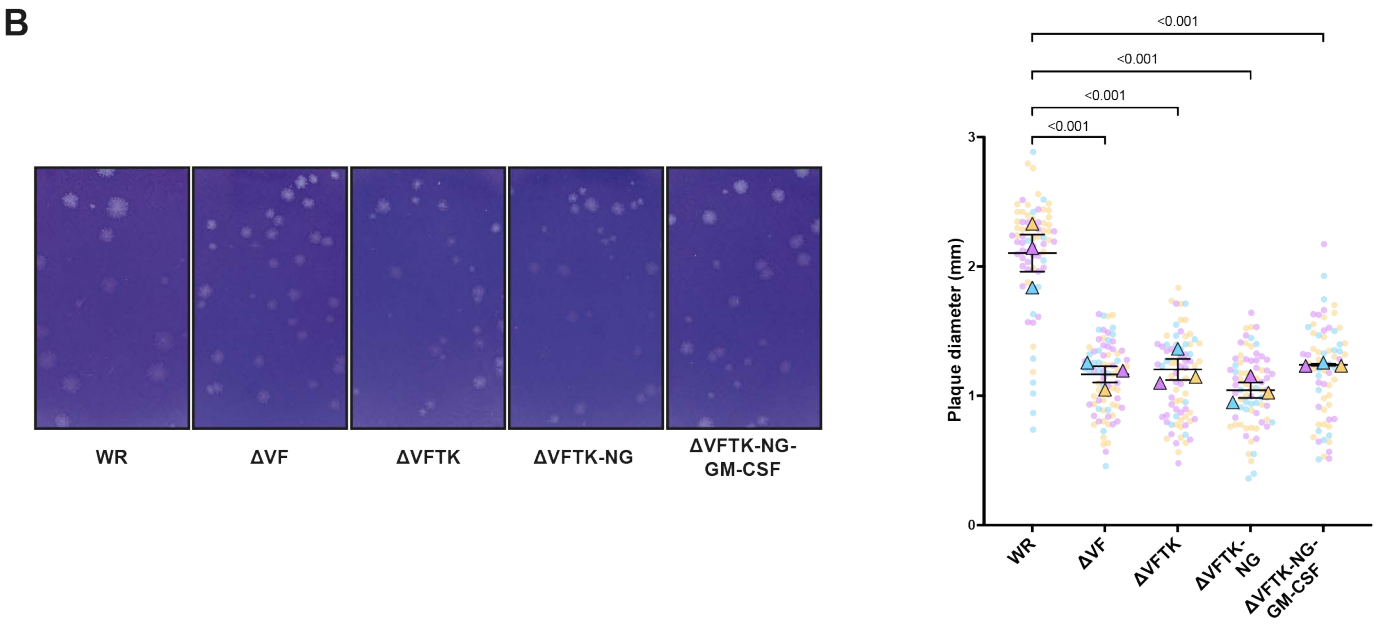
B
WR
ΔVF
ΔVFTK
ΔVFTK-NG
ΔVFTK-NG-GM-CSF
<0.001
<0.001
<0.001
<0.001
Plaque diameter (mm)
0
1
2
3
WR
ΔVF
ΔVFTK
ΔVFTK-NG
ΔVFTK-NG-GM-CSF

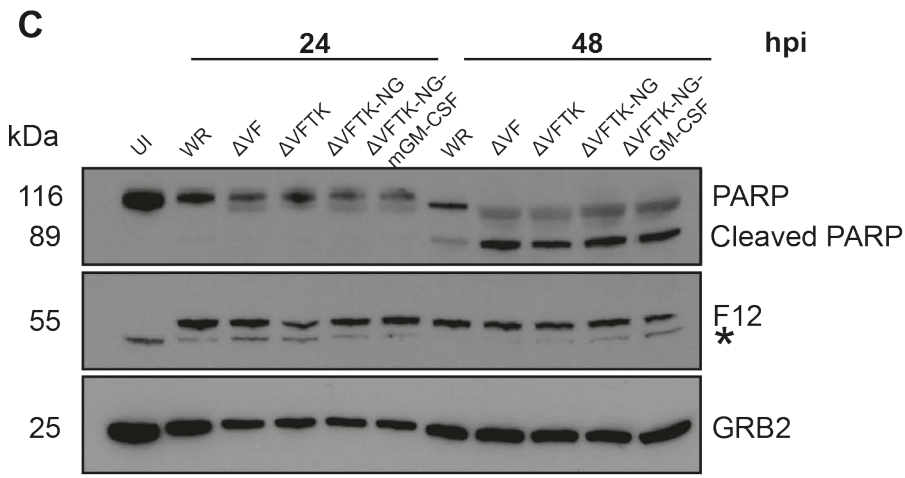
C
24
48
hpi
kDa
UI
WR
ΔVF
ΔVFTK
ΔVFTK-NG
ΔVFTK-NG-mGM-CSF
WR
ΔVF
ΔVFTK
ΔVFTK-NG
ΔVFTK-NG-GM-CSF
116
89
PARP
Cleaved PARP
55
F12
*
25
GRB2

Figure 1

A

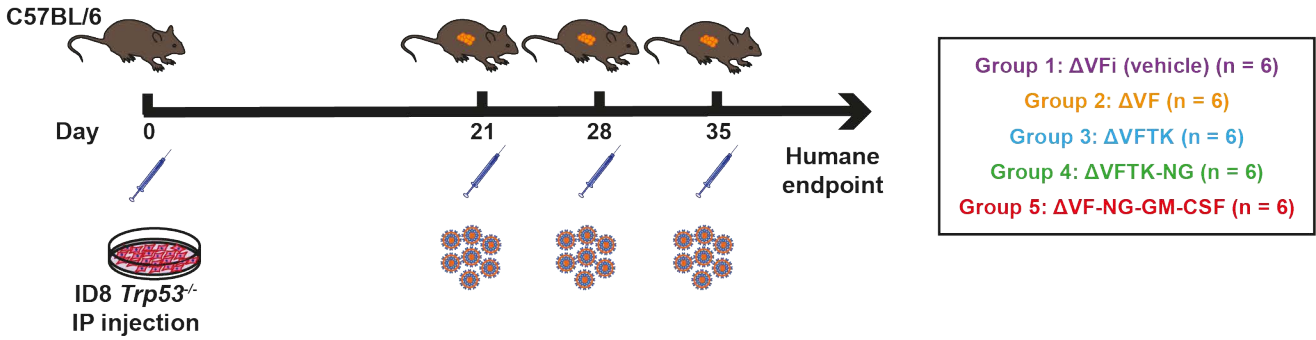

B

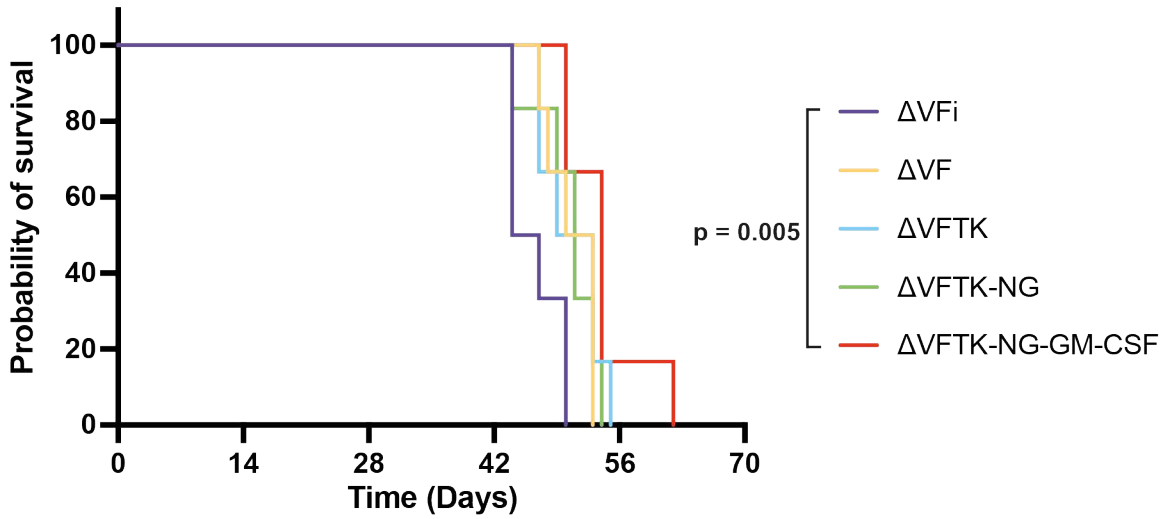

C

	ΔVFi	ΔVF	ΔVFTK	ΔVFTK-NG	ΔVFTK-NG-GM-CSF
Omental tumour (mg)	135.0 ± 51.0	116.0 ± 45.0	106.0 ± 20.0	84.0 ± 28.0	81.0 ± 15.0
Spleen (mg)	266.0 ± 95.0	264.0 ± 57.0	285.0 ± 50.0	243.0 ± 43.0	219.0 ± 104.0
Liver (mg)	815.2 ± 130.9	877.2 ± 146.9	842.0 ± 202.0	817.2 ± 117.6	776.5 ± 139.4
Ascites (ml)	4.1 ± 1.8	4.5 ± 2.4	2.5 ± 0.5	3.0 ± 1.1	3.0 ± 0.6

Figure 2

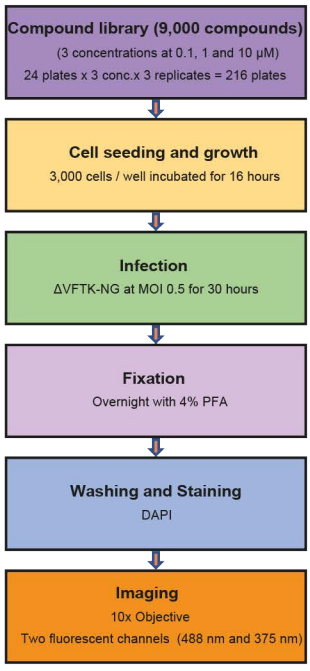

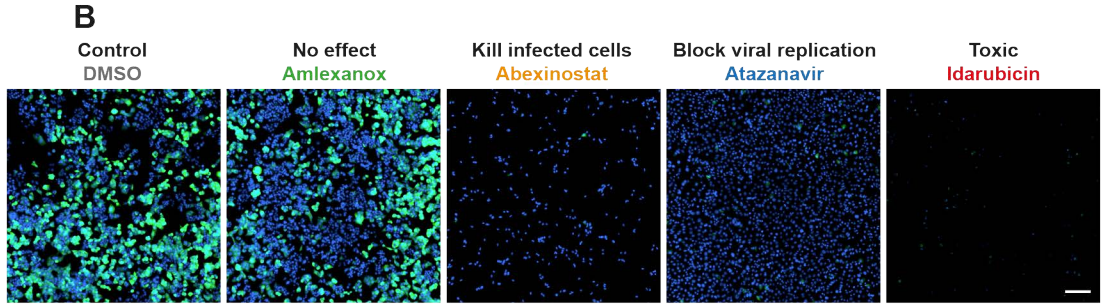

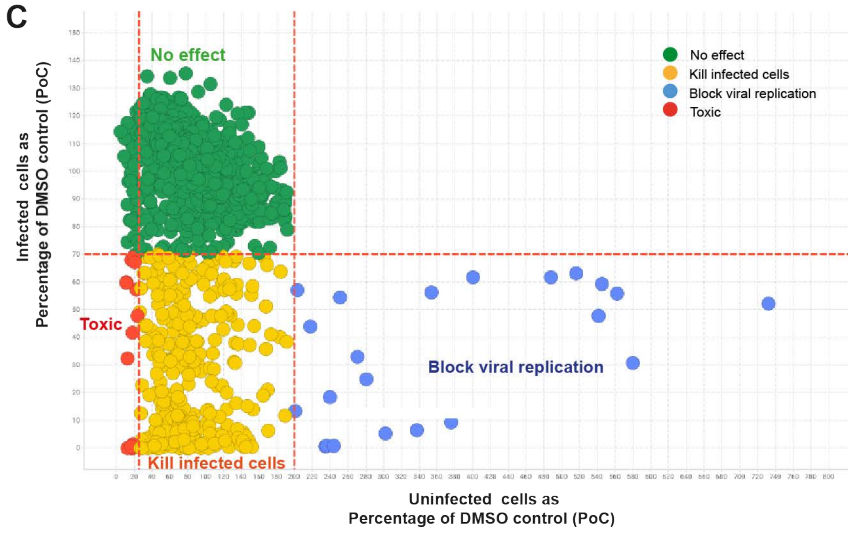

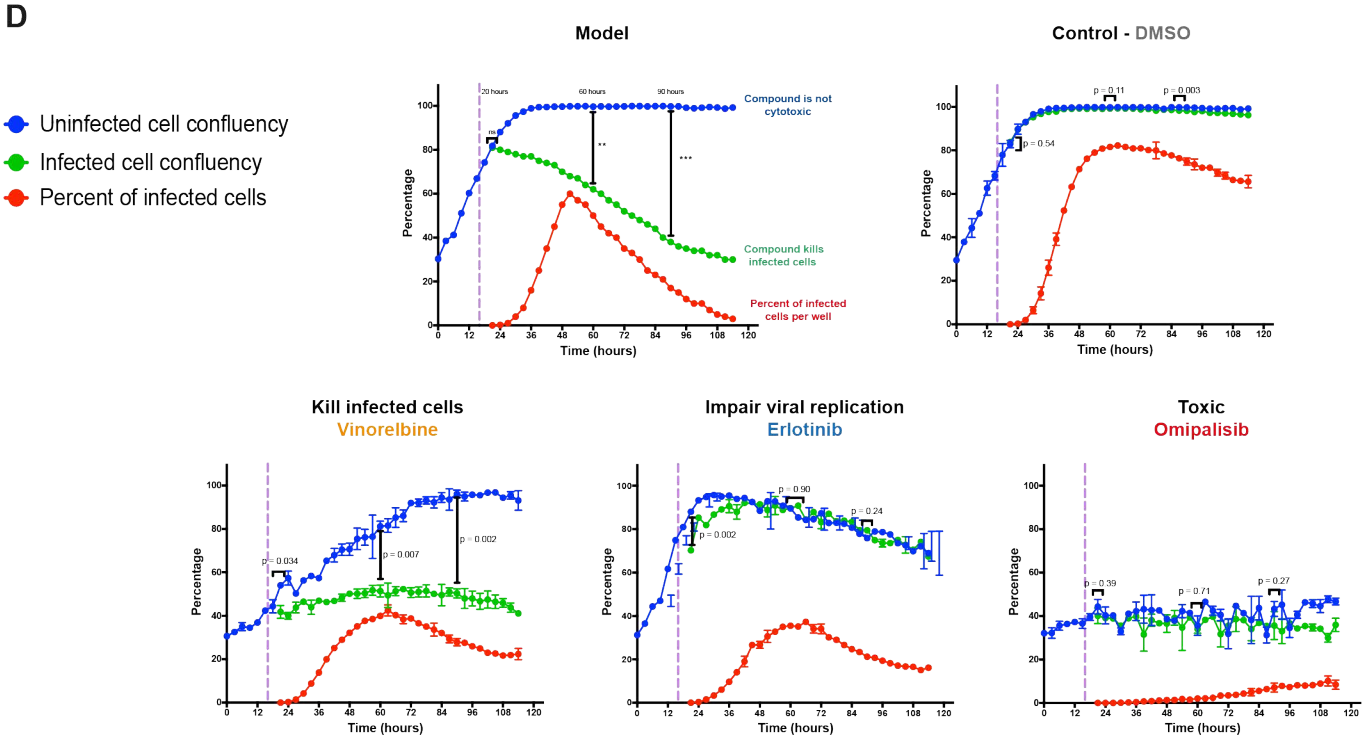

E

Drug	Mechanism of action
5-Fluorouridine	Pyrimidine nucleoside analogue
Abexinostat	Pan-histone deacetylase inhibitor
Aminopterin	Dihydrofolate reductase inhibitor
Auristatin F	**Tubulin polymerisation inhibitor**
CHIR-124	Selective Chk 1 inhibitor
Combretastatin A4	**Tubulin polymerisation inhibitor**
Cytarabine	Pyrimidine nucleoside analogue
Ellipticine	Type II topoisomerase inhibitor
Erastin	Ferroptosis inhibitor
Geldanamycin	HSP 90 inhibitor
Gemcitabine	Nucleoside (cytidine analogue) metabolic inhibitor
IMD-0345	IKKβ inhibitor
JNJ-10198498	Platelet-derived growth factor receptor inhibitor
MMAF hydrochloride	**Tubulin polymerisation inhibitor**
Nonactin	Ionophore for monovalent cations, uncouples oxidative phosphorylation of mitochondria
Sepantronium (bromide)	Survivin inhibitor
SPDB-DM4	**DM4 (tubulin inhibitor) is a maytansine-derived payload linked via an SPDB linker**
Tubulin inhibitor	**Tubulin polymerisation inhibitor**
Vinblastine	**Tubulin polymerisation inhibitor**
Vinorelbine	**Tubulin polymerisation inhibitor**

Figure 3

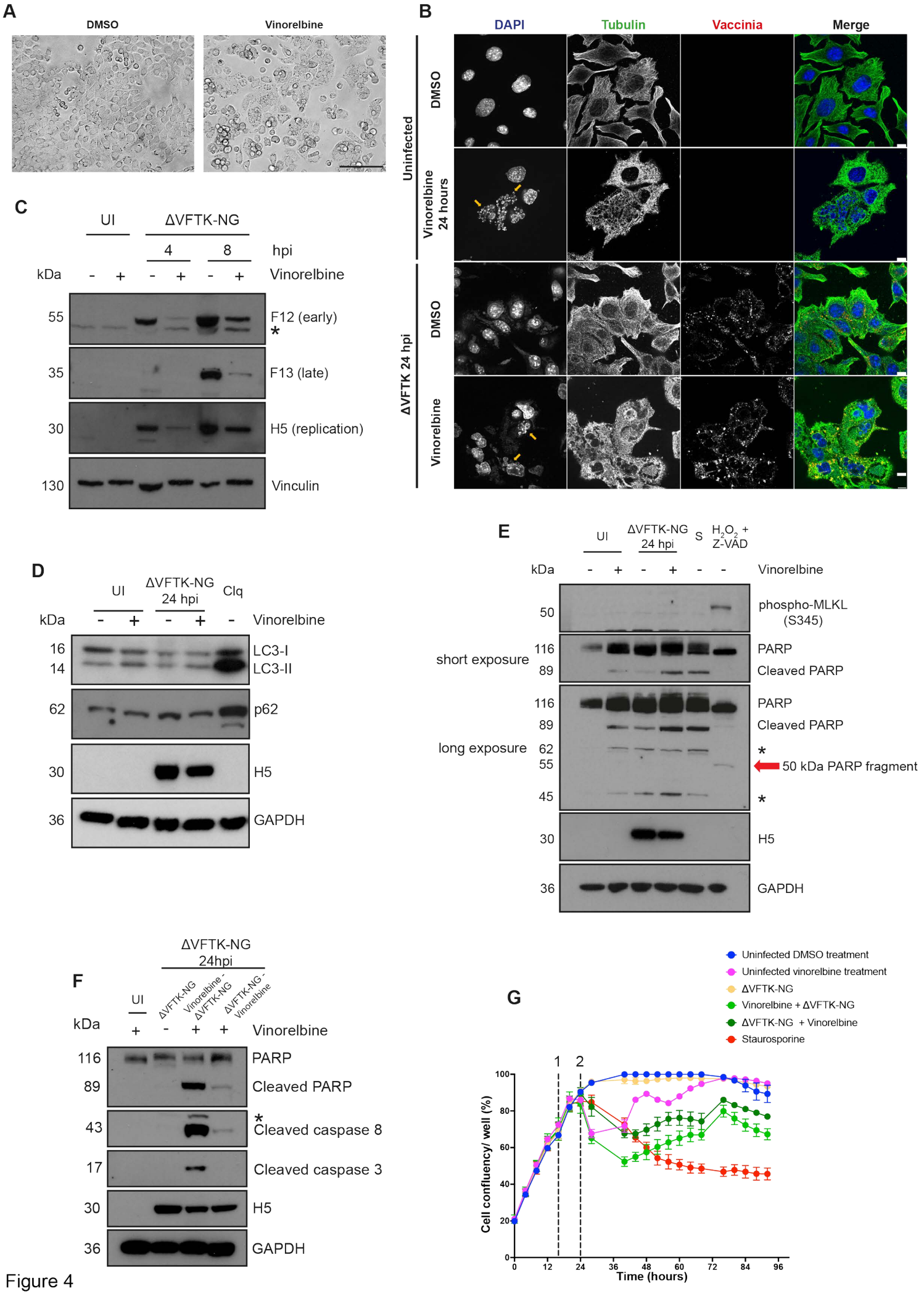
A
DMSO
Vinorelbine
B
DAPI
Tubulin
Vaccinia
Merge
Uninfected
DMSO
Vinorelbine 24 hours
ΔVFTK 24 hpi
DMSO
Vinorelbine
C
UI
ΔVFTK-NG
4
8
hpi
kDa
Vinorelbine
55
F12 (early)
*
35
F13 (late)
30
H5 (replication)
130
Vinculin
D
UI
ΔVFTK-NG 24 hpi
Clq
kDa
Vinorelbine
16
14
LC3-I
LC3-II
62
p62
30
H5
36
GAPDH
E
UI
ΔVFTK-NG 24 hpi
S
H2O2 + Z-VAD
kDa
Vinorelbine
50
phospho-MLKL (S345)
short exposure
116
89
PARP
Cleaned PARP
long exposure
116
89
62
55
45
PARP
Cleaned PARP
*
50 kDa PARP fragment
*
30
H5
36
GAPDH
F
ΔVFTK-NG 24hpi
UI
ΔVFTK-NG
Vinorelbine - ΔVFTK-NG
ΔVFTK-NG - Vinorelbine
kDa
Vinorelbine
116
PARP
89
Cleaved PARP
43
*
Cleaved caspase 8
17
Cleaved caspase 3
30
H5
36
GAPDH
G
Uninfected DMSO treatment
Uninfected vinorelbine treatment
ΔVFTK-NG
Vinorelbine + ΔVFTK-NG
ΔVFTK-NG + Vinorelbine
Staurosporine
1
2
Cell confluency/ well (%)
Time (hours)

Figure 4

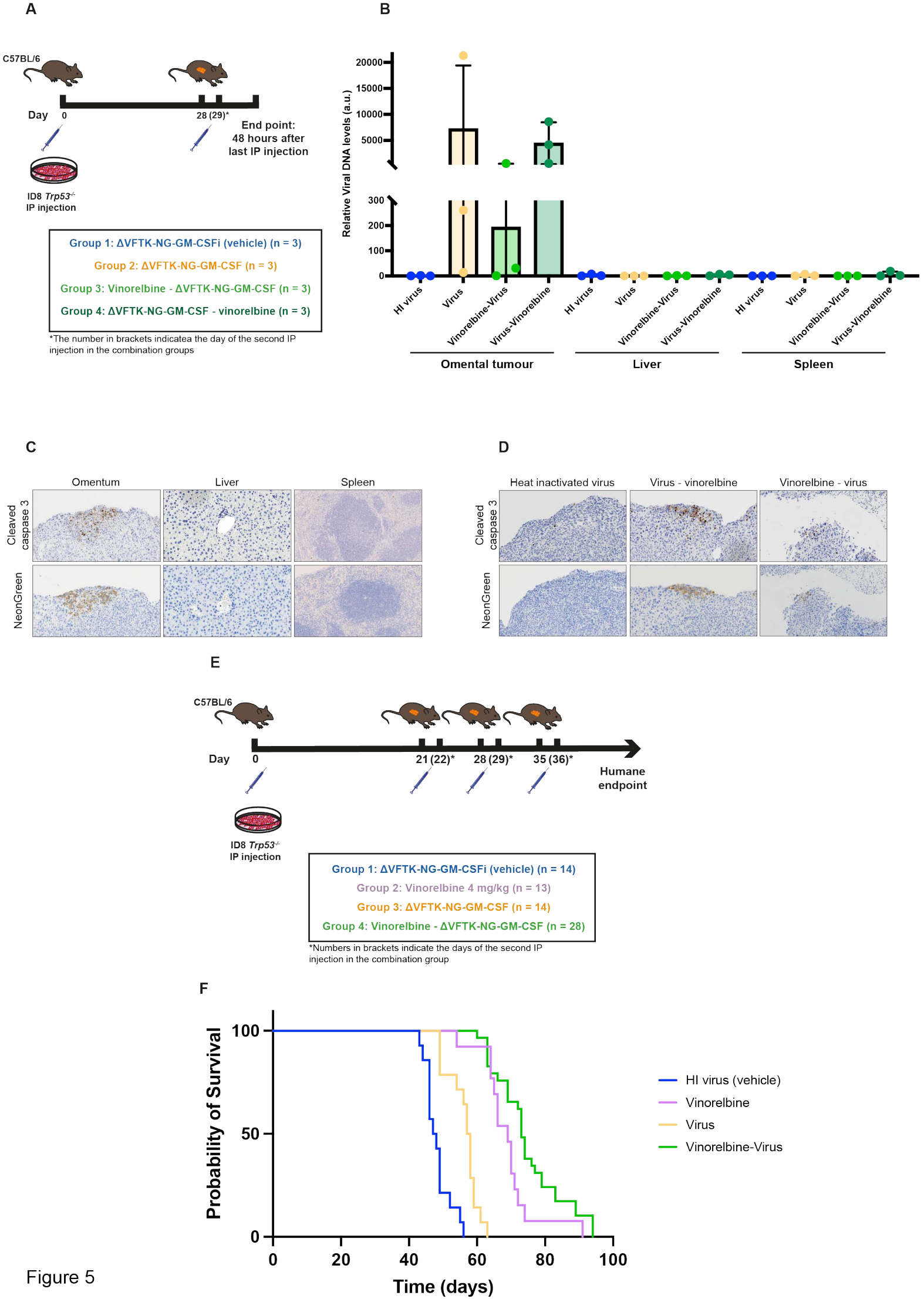
A
C57BL/6
Day 0
28 (29)*
End point:
48 hours after
last IP injection
ID8 Trp53-/-
IP injection
Group 1: ΔVFTK-NG-GM-CSFi (vehicle) (n = 3)
Group 2: ΔVFTK-NG-GM-CSF (n = 3)
Group 3: Vinorelbine - ΔVFTK-NG-GM-CSF (n = 3)
Group 4: ΔVFTK-NG-GM-CSF - vinorelbine (n = 3)
*The number in brackets indicatea the day of the second IP injection in the combination groups
B
Relative Viral DNA levels (a.u.)
20000
15000
10000
5000
300
200
100
0
HI virus
Virus
Vinorelbine-Virus
Virus-Vinorelbine
Omental tumour
Liver
Spleen
C
Omentum
Liver
Spleen
Cleaved caspase 3
NeonGreen
D
Heat inactivated virus
Virus - vinorelbine
Vinorelbine - virus
Cleaved caspase 3
NeonGreen
E
C57BL/6
Day 0
21 (22)*
28 (29)*
35 (36)*
Humane endpoint
ID8 Trp53-/-
IP injection
Group 1: ΔVFTK-NG-GM-CSFi (vehicle) (n = 14)
Group 2: Vinorelbine 4 mg/kg (n = 13)
Group 3: ΔVFTK-NG-GM-CSF (n = 14)
Group 4: Vinorelbine - ΔVFTK-NG-GM-CSF (n = 28)
*Numbers in brackets indicate the days of the second IP injection in the combination group
F
Probability of Survival
100
50
0
0
20
40
60
80
100
Time (days)
HI virus (vehicle)
Vinorelbine
Virus
Vinorelbine-Virus

Figure 5